Allosteric modulation of human melanocortin-4 receptor (MC4R) by zinc and copper ions and characterization of spotted sea bass MC4R

By

Zhi-Shuai Hou

A dissertation submitted to the Graduate Faculty of
Auburn University
in partial fulfillment of the
requirements for the Degree of
Doctor of Philosophy

Auburn, Alabama
August 8, 2020

Keywords: G protein-coupled receptor, Melanocortin-4 receptor, Allosteric modulator, Energy homeostasis, Fish

Approved by

Ya-Xiong Tao, Chair, Professor of Physiology
Benson T. Akingbemi, Professor of Veterinary Anatomy
Ramesh B. Jeganathan, Professor of Nutrition
Chen-Che “Jeff” Huang, Assistant Professor of Pharmacology

Abstract

Since the metal ions have been shown to play an important role in regulating signal transduction of G protein-coupled receptors (GPCRs), we investigated whether the Zn^{2+} and Cu^{2+} regulate the pharmacology of human melanocortin-4 receptor (hMC4R). We showed Zn^{2+} and Cu^{2+} were not able to displace ^{125}I-NDP-MSH but exerted allosteric effects on the binding affinities and signaling properties of endogenous agonist (α-melanocyte stimulating hormone, α-MSH) at hMC4R. In addition, Zn^{2+} and Cu^{2+} induced biased signaling at hMC4R as they selectively modulated the canonical cAMP signaling but failed to regulate the ERK1/2 signaling. Notably, Cu^{2+} stimulated a biphasic cAMP accumulation not only at wild-type (WT) but also at obesity-associated gain-of-function mutant MC4Rs, suggesting this biphasic action might constitute as novel therapeutic opportunities for obese patients with these mutations. We also showed the Zn^{2+} cannot influence RM493 (a second-generation of MC4R agonist)-induced cAMP accumulation at WT and rescued loss-of-function mutant MC4Rs. This is probably due to the fact that the histidine residue of central amino acid motif (His-Phe-Arg-Trp) of RM493 and α-MSH coordinate with hMC4M at different binding pockets. Compared to WT hMC4R, the D122A, a “WT-like” variant, exerted significantly decreased cAMP producing in response to Zn^{2+}, suggesting D122, the binding site of calcium, also serves as a potential binding site of Zn^{2+} at hMC4R. Our study might provide novel therapeutic applications for repurposing or designing drugs with metal ions combining allosteric and biased properties.

The MC4R plays important roles in regulation of multiple physiological processes including energy homeostasis, reproduction, sexual function and other functions in mammals. Recent studies suggested that teleost MC4Rs have different physiological functions and pharmacological characteristics when compared to mammalian MC4Rs. In this study, we investigated spotted sea bass (*Lateolabrax maculatus*) MC4R (*Lm*MC4R) physiology and pharmacology. Spotted sea bass *mc4r* consisted of a 984 bp open reading frame encoding a protein of 327 amino acids. *Lm*MC4R was homologous to those of several teleost MC4Rs and hMC4R. qRT-PCR and *in situ* hybridization revealed that *mc4r* transcripts were highly expressed in the brain, followed by pituitary and liver. Brain *mc4r* transcripts were down-regulated in long-term and short-term fasting challenges. *Lm*MC4R was a functional receptor with lower maximal binding and higher basal activity than hMC4R. AgRP could displace ^{125}I-NDP-MSH and serve as the inverse agonist. THIQ, Ipsen 5i and ML00253764 were not able to displace ^{125}I-NDP-MSH but could affect intracellular cAMP accumulation, suggesting that they were allosteric ligands for *Lm*MC4R. In summary, we cloned spotted sea bass MC4R, and showed that it had different pharmacological properties compared to hMC4R, and potentially different functions.

In summary, we showed Zn^{2+} and Cu^{2+} served as biased allosteric modulators at hMC4R. We also investigated the physiology and pharmacology of spotted sea bass MC4R.

Acknowledgments

I would like to express my deepest gratitude to my mentor, Dr. Ya-Xiong Tao, who has provided me with the outstanding opportunity to study abroad as a PhD student with great support, continuous guidance and inexhaustible patience. It is really an honor for both of me and my family. This dissertation would not be done without his meticulous suggestions and constant encouragements.

I would like to sincerely appreciate my graduate committee members, Drs. Benson Akingbemi, Ramesh Jeganathan, and Huang Chen-Che “Jeff” for sharing their wisdom, experience, advice, and expertise during the past four years. I am thankful to my university reader Dr. Michael Greene for his careful review and precious suggestions.

I would like to thank my lab colleagues and alumni, Chuan-Ling Xu, Ting Liu, Ren-Lei Ji, Drs. Wei Wang, Li-kun Yang, Qian Wang and Fan Yu, for their valuable contributions to my work. I would like to thank all the faculty and staff members and students in the Department of Anatomy, Physiology and Pharmacology. Specifically, I would like to acknowledge China Scholarship Council of the People’s Republic of China for the financial support throughout these years. I would like to acknowledge the Ocean University of China for the financial support.

I would like to express my sincere appreciation to my first mentor, Dr. Hai-Shen Wen,

who have provided strong support for my graduate work in Auburn University. I would like to thank my supervisors, lab colleagues and alumni in Ocean University of China, Mrs. Shu-Guang Wang, Ji-Fang Li; Drs. Qi Li, Xie-Fa Song, Qing-Feng Gao, Feng He, Yun Li, Xin Qi, Kai-Qiang Zhang; and Yuan Tian, Hong-Long Wang, Yuan-Ru Xin, Chu Zeng and Hong-Kui Zhao. I would like to thank all the faculty and staff members and students in the Fishery College of Ocean University of China.

Finally, I am grateful to my loved parents for their unconditional and endless love, encouragement, and tremendous support.

Table of Contents

List of Tables

List of Figures

List of Abbreviations

ACTH, adrenocorticotropic hormone;

AgRP, Agouti-related peptide;

AMPK, 5'-AMP-activated protein kinase;

ARC, arcuate nucleus;

CREB, cAMP response element-binding protein;

CNS, central nervous system;

ddH_2O, double-distilled water;

DMH, dorsomedial nucleus of the hypothalamus;

ECL, extracellular loop;

ER, endoplasmic reticulum;

FBS, fetal bovine serum;

GABA, γ-aminobutyric acid;

GPCR, G protein-coupled receptor;

GRKs, G-protein-coupled receptor kinases;

HEK 293T cells, human embryonic kidney 293T cells;

hMC4R, human MC4R;

HPA, hypothalamus-pituitary-adrenal;

i.c.v, intracerebroventricular;

ICL, intracellular loop;

IML, intermediolateral nucleus of the spinal cord;

JNK, c-Jun N-terminal kinases;

MCR, melanocortin receptor;

MSH, melanocyte-stimulating hormone;

NDP-MSH, [Nle^4, D-Phe^7]-α-MSH;

NPY, neuropeptide Y;

NTS, nucleus tractus solitarius;

ORF, open reading frame;

PBS, phosphate buffered saline;

PKA/C, protein kinase A/C;

PKB or AKT, protein kinase B;

PLC, phospholipase C;

POMC, proopiomelanocortin;

PTX, pertussis toxin;

PVN, paraventricular nucleus;

RhoGEFs, Rho guanine nucleotide exchange factors;

THIQ, N-[(3R)-1,2,3,4-tetrahydroisoquinolinium-3-ylcarbonyl]-(1R)-1-(4-chlorobenzyl)-2-[4-cyclohexyl-4-(1H-1,2,4-triazol-1-ylmethyl)piperidin-1-yl]-2-oxoethylamine;

TMD, transmembrane domain;

WT, wild-type;

α-, β-,and γ-melanocyte stimulating hormone (α-, β-, and γ-MSH).

Chapter 1: Literature review

1.1. Introduction

G protein-coupled receptors (GPCRs) are the largest family of the membrane receptors located in both plasma and intracellular membranes [1, 2]. With more than 1000 identified members in humans, GPCRs transduce the extracellular signals and regulate almost all physiological functions [3]. For example, the senses of the outside environment, including the vision, smell and taste, are modulated by sensory GPCRs that could be activated by light, odorants or tastes [4, 5]. GPCRs also regulate intercellular signals, converting extracellular signals from first messages such as neuropeptides, catecholamines, lipids, amino acids, hormones and metal ions, into intracellular second signals [3, 4].

Melanocortins are important in regulating immunomodulation, steroidogenesis, energy balance and lipid metabolism and these hormones exhibit their physiological functions by activating melanocortin receptors (MCRs) [6]. MCRs belong to Family A rhodopsin-like GPCRs and five MCRs, named MC1R to MC5R, have been identified in mammals [6, 7]. MC1R is highly expressed in skin, hair and immune cells and regulates pigmentation and immunomodulation [8]. MC2R is the ACTH receptor and plays an important role in modulating steroidogenesis and hypothalamus-pituitary-adrenal (HPA) axis [9]. MC3R and MC4R are highly expressed in central nervous system (CNS) and named neural MCRs [6, 7]. MC3R and MC4R exhibit non-redundant roles in regulating

energy homeostasis [10]. In addition to energy balance, neural MCRs are also involved in regulations of cardiovascular function, reproduction and immunomodulation [6, 11, 12]. MC5R is primarily expressed in exocrine gland and regulates the exocrine gland secretion [13].

This chapter provides a literature review of the physiology and pharmacology of central melanocortin systems. The regulation of energy homeostasis by central melanocortin system is discussed. The intracellular signal transduction triggered by neural MCRs are also highlighted.

1.2. The central melanocortin system

1.2.1 Endogenous ligands

The melanocortin system consists of four known endogenous agonists and two endogenous antagonists. The four endogenous agonists, including α-, β-, and γ-melanocyte-stimulating hormones (α-, β-, and γ-MSH) and adrenocorticotropic hormone (ACTH), are produced by posttranslational processing of proopiomelanocortin (POMC) (reviewed in [14, 15]). The POMC neurons are primarily located in the arcuate nucleus (ARC) in the hypothalamus, with a small POMC populations expressing in the nucleus tractus solitarius (NTS) of the brainstem [14]. The melanocortin system is unique because two endogenous antagonists, named Agouti and Agouti-related peptide (AgRP), are

identified [6].

The α-, β-, γ-MSH or ACTH exhibits different specificities to MCRs. The α-MSH and β-MSH show agonist activities at MC1R, MC3R, MC4R and MC5R and the γ-MSH exerts modest selectivity at MC3R. The α-, β-, and γ-MSH fail to activate MC2R while ACTH results in activation of MC2R [16]. Agouti selectively binds to MC1R and MC4R as endogenous antagonist [17, 18], whereas AgRP specifically functions as antagonist at MC3R and MC4R [19, 20]. Recent studies further showed that AgRP serves as an inverse agonist at MC3R and MC4R, suppressing the constitutive (basal) activities [6, 21, 22].

1.2.2. Physiological functions of central melanocortin system in energy homeostasis

Energy homeostasis, which refers to biological processes that coordinate the energy intake and energy expenditure over a prolonged time, is important to maintain the long-term stability of the energy storage in organism [23]. Energy homeostasis not only regulates the normal energy expenditure, which is consumed by daily behavior and regular physiology, but also monitors the energy storage, which is essential for survival, development, growth and reproduction with low food intake availability [23]. Energy (food) intake is regulated by several external factors, such as temperature, stress, food availability, as well as multiple internal factors including genetic information, development stages, metabolite and hormone levels [24-27]. Hypothalamus is the hub that integrates these signals and controls energy homeostasis [28]. For example, in the ARC of the

hypothalamus, leptin, which is released by adipocyte [29], activates the leptin receptors located in orexigenic neurons expressing neuropeptide Y (NPY) and Agouti-related peptide (AgRP), and further decreases appetite by suppressing AgRP releasing [6, 23, 28]. Meanwhile, leptin binds to the receptors on anorexigenic neurons expressing POMC, resulting in α-MSH release [6, 23, 28]. The enhanced α-MSH and reduced AgRP cooperatively regulate the neurons expressing MC3R and MC4R in hypothalamic paraventricular nucleus (PVN), thus regulating energy homeostasis [6, 23, 28].

Mouse genetic studies showed MC3R regulates feeding efficiency and fat storage, but do not regulate food intake. For example, the *Mc3r* knockout mice did not exhibit hyperphagia and obesity when compared to the wild-type (WT) littermates; these *Mc3r* knockout mice showed normal energy expenditure and even decreased food intake [10, 30]. However, the *Mc3r* knockout mice showed increased fat mass and reduced lean mass [10]. Mice lacking both MC3R and MC4R exhibited exacerbated obesity when compared with MC3R or MC4R single gene knockout mice, further showing that MC3R and MC4R have non-redundant functions in regulating energy homeostasis [10]. In human genetic studies, a potential loss-of-function *MC3R* mutation was identified from two obese patients in 2002 [31]. The following studies convinced that this mutant fails to convey ligand binding to $G\alpha_s$ signaling activation [32]. Sequentially, several novel MC3R variants were identified form subjects who had increased fat mass and decreased lean mass [33]. A recent study showed novel functions of MC3R in regulating rheostatic and boundary control on energy storage via melanocortin signaling [34]. The MC3R expressing in AgRP neurons could exert inhibitory signaling to MC4R by modulating γ-

aminobutyric acid (GABA) release onto anorexigenic MC4R neurons, thus regulating upper and lower boundaries of energy homeostasis [34].

The *Mc4r* knockout mice showed hyperphagia and decreased energy expenditure, indicating MC4R primarily regulates food intake and energy expenditure [35]. Food intake accounts for 60% of the physiological functions of MC4R in energy homeostasis and the remaining 40% of the MC4R functions regulate energy expenditure [36]. Mouse genetic studies further showed MC4R expressing neurons regulate food intake in PVN and amygdala of hypothalamus, while modulate energy expenditure in intermediolateral nucleus of the spinal cord (IML) and dorsomedial nucleus of the hypothalamus (DMH) [36-38]. In human genetic studies, two groups independently identified frameshift *MC4R* mutations from patients with early-onset obesity in 1998 [39, 40], showing that MC4R is important in regulating energy homeostasis. After that, more than 170 distinct *MC4R* mutations associated with obesity and other diseases have been identified from patients in different cohorts from Asia, Europe and North America [6].

1.2.3. Multiple signaling pathways of MC3R and MC4R

The canonically intracellular signaling of GPCRs is regulated by heterotrimeric G proteins consisting of two functional units: an α subunit and a $\beta\gamma$ dimer. In the absence of the ligands, the heterotrimeric G protein is inactivated and the GDP-attached α subunit is tightly associated with the $\beta\gamma$ dimer [41]. Binding of a signaling molecule to the receptor could activate the G protein with conformational changes, thus triggering the substitution

of GTP for GDP on the α-subunit and the dissociation of α-subunit from $\beta\gamma$ dimer [42].

The GTP-bound α-subunit could activate multiple signaling proteins, thereby regulating the intracellular signal transduction pathways via second messengers of cyclic AMP (cAMP), inositol 1,4,5-trisphosphate (IP3), diacylglycerol (DAG) and calcium (Ca^{2+}). Based on structural and functional similarity, the α-subunits could be broadly divided into four subtypes of stimulatory G protein ($G\alpha_s$), inhibitory G protein ($G\alpha_i$), $G\alpha_q$ and $G\alpha_{12/13}$ [43, 44]. The $G\alpha_s$ protein could activate the adenylyl cyclase, resulting in increased cAMP concentrations and subsequently activation of protein kinase A (PKA). The $G\alpha_i$ inhibits the production of the cAMP. The PKA could activate the functional proteins targeted in cytoplasm and membrane, thus regulating the cellular functions via a faster non-genomic signaling. The PKA also activate the proteins targeted in the nucleus (such as the cAMP response element-binding protein (CREB)) and modulate the cellular functions via a slower genomic signaling [45]. Activation of $G\alpha_q$ could increase the intracellular inositol IP3 and DAG via activating phospholipase C (PLC). IP3 activates the release of Ca^{2+} from endoplasmic reticulum (ER) and the DAG and IP3-induced Ca^{2+} can activate protein kinase C (PKC), thus regulating enzyme activities, metabolic pathways and gene expressions. The $G\alpha_{12/13}$ subtype specifically target Rho guanine nucleotide exchange factors (RhoGEFs) and activates the RhoA kinase. In addition to the α-subunit-regulated second messengers signaling pathway, the $\beta\gamma$ dimer and other proteins (such as β-arrestins) could also trigger the down-stream signaling pathway and modulate the cellular functions [46-49].

In addition to the G protein-dependent signaling, GPCRs also exert G protein-independent signaling transduction [46]. Following agonist binding and phosphorylation of receptors by G-protein-coupled receptor kinases (GRKs), the G protein coupling is typically terminated by the recruitment of β-arrestins (β-arrestin-1 or β-arrestin-2), which is termed as GPCR desensitization [46, 50]. The β-arrestins can also serve as the adaptors that target GPCRs to clathrin-coated pits for internalization. In addition to attenuating GPCRs signaling, recent studies revealed that β-arrestins also function as scaffolding molecules to trigger intracellular signaling including mitogen-activated protein kinases (MAPKs) signaling [46, 50].

The canonical signaling pathway of MC3R is to couple $G\alpha_s$ signaling [51]. The MC3R activation results in enhanced cAMP accumulation and consequently PKA activation. The MC3R is also reported to activate $G\alpha_i$ and $G\alpha_q$ signaling pathways [52, 53]. Konda et al. showed MC3R regulates intracellular calcium mobilization via the IP3-dependent signaling, suggesting MC3R activates the $G\alpha_q$ signaling [53]. In MC3R-transfected HEK293 cells, the NDP-MSH, a super potent analogue of α-MSH, can activate the $G\alpha_i$ signaling and extracellular signal-regulated kinases 1/2 (ERK1/2) signaling [52]. Noticeably, NDP-MSH triggers the ERK1/2 signaling via $G\alpha_i$-PI3K signaling rather than PKA, PKC and Ca^{2+} signaling [52], while AgRP, the inverse agonist of MC3R, activates ERK1/2 signaling in a PKA or PI3K-independent manner [54], suggesting the MC3R shows cell-specific and ligand-specific mechanism of ERK1/2 activation.

The conventual signaling of MC4R is by coupling to $G\alpha_s$-cAMP-PKA pathway [6]. In

addition, MC4R activation has been shown to activate the $G\alpha_i$ and $G\alpha_q$ signaling pathways [55, 56]. In GT1-7 cells, a mouse hypothalamic cell line endogenously expressing MC4R, the α-MSH-induced G protein activation (measured by radiolabeled non-hydrolysable GTP analog, GTPγS35) can be partially (~50%) blocked by $G\alpha_i$ inhibitor (pertussis toxin, PTX). and the intracellular cAMP level triggered by α-MSH is enhanced (~150%) with PTX [55]. These results indicate that the endogenous agonist, α-MSH, activates $G\alpha_s$ and $G\alpha_i$ signaling simultaneously [55]. AgRP, an inverse agonist of MC4R, could antagonize the $G\alpha_s$ activation and activate $G\alpha_i$ signaling, thereby decreasing the basal activity [55]. The MC4R activation also couples to $G\alpha_q$ signaling pathway [56]. Another study using GT1-1 cells, another mouse hypothalamic cell line endogenously expressing MC4R, showed MC4R activation results in increased intracellular calcium via $G\alpha_q$-PLC signaling pathway [56]. However, the MC4R fails to activate the $G\alpha_q$-PLC signaling in GT1-7 cell line [55], suggesting that activation of $G\alpha_q$ signaling through MC4R varies based on cell types and probably ligands types.

Multiple *in vitro* and *in vivo* studies showed MC4R-mediated ERK1/2 activation, although the specific activation mechanisms are different based on cell types [57, 58]. For example, NDP-MSH results in ERK1/2 activation via $G\alpha_i$ signaling in HEK293 cells expressing MC4R [57], or via PI3K-regulated signaling in CHO cells stably expressing MC4R [59]. In cell lines endogenously expressing MC4R, NDP-MSH activates ERK1/2 signaling via Ca^{2+}- and PKC-dependent signaling in GT1-1 cells, or PKA-dependent signaling in GT1-7 cells [57, 60]. Although the β-arrestin-activated ERK1/2 signaling or endocytosis was observed in MCRs [61-63], and even a recent study revealed MC4R

mutants that cause enhanced β-arrestin recruitment rather than increased cAMP production contribute to increased ERK1/2 activation [64], there is no directly evidence of β-arrestin-activated ERK1/2 signaling in MC4R. In addition to ERK1/2 signaling, activation of the MC4R are also involved in other signaling pathways, including c-Jun N-terminal kinases (JNK), 5'-AMP-activated protein kinase (AMPK), and protein kinase B (PKB or AKT) signaling pathways [52, 54, 59, 60, 65, 66].

Chapter 2: Allosteric modulation of human melanocortin-4 receptor by zinc and copper ions

2.1. Introduction

Metal ions, which are involved in multiple processes of human physiology, are reported to interact with different types of membrane proteins including ion channels [67], ionotropic receptors [68, 69] and GPCRs [1, 70]. Zn^{2+} is an important trace element and plays an important role in the functioning of the whole body [71]. The zinc is stored with high concentrations (~hundreds μM) in nerve terminals and co-released with neurotransmitters [72, 73]. Zn^{2+} binds to membrane proteins particularly in neurons, including ion channels, membrane transporters and receptors (reviewed in [74]). Indeed, Zn^{2+} shows higher binding affinity to the thiol group of cysteine, aromatic nitrogen of histidine and carboxy group of aspartate and glutamate. For example, the Zn^{2+} acts as the natural ligand at GPR39 by directly binding to His^{17} and His^{19} located in the extracellular domain and [75]. In addition to GPR39, previous studies also reported that Zn^{2+} allosterically modulate MC1R. Alignment of the amino acid sequences between MC1R and MC4R showed that the binding sites of Zn^{2+} are conserved, indicating Zn^{2+} is a potential ligand or modulator of MC4R [74, 76].

In addition to Zn^{2+}, copper is also reported to be stored in brain with higher concentrations (~70 μM) and interacts with proteins through the same mechanism as Zn^{2+} [77]. For example, both copper ions (Cu^{2+}) and Zn^{2+} can interact with the aromatic

nitrogen of histidines in Cu, Zn-superoxide dismutase (Cu, Zn-SOD), thereby stabilizing the protein conformation [78]. In membrane proteins, Cu^{2+} is reported to block the γ-aminobutyric acid subtype A (GABAA) receptors with the similar mechanism of Zn^{2+} [79-81]. An early study showed Cu^{2+} could displace the radioactive labeled ligand (^{125}I-NDP-MSH) at mouse MC1R and human MC4R, but fail to activate the receptors [74]. However, a recent study showed Cu^{2+} exerts biphasic effect in activating cAMP signaling at hMC4R [82].

The human *MC4R*, which is first cloned in 1993, is an intronless gene located at chromosome 18q21.3 that encodes a protein of 332 amino acids [83, 84]. The *MC4R* mRNA is primarily expressed in the CNS, including the cortex, thalamus, hippocampus, hypothalamus, brain stem, and spinal cord, and involved in regulating food intake and energy expenditure [84-86]. For example, intracerebroventricular (ICV) administration of MC4R agonists, such as α-MSH and ACTH, reduces food intake in rats [87, 88], while deletion of mice *Mc4r* results in maturity onset obesity with hyperphagia, hyperinsulinemia, and hyperglycemia [35]. Human genetic studies further convinced that MC4R is associated with pathophysiology of obesity. In 1998, two groups independently reported that the frameshift mutations of the *MC4R* gene cause severe early-onset obesity [39, 40]. After that, more than 170 *MC4R* gene mutations are reported to be involved in obesity and other diseases in patient cohorts of different ethnic origins [6].

Extensive functional studies showed that the majority of the MC4R mutants belong to loss-of-function mutants and they are retained intracellularly (Reviewed in [89] and [90]).

These mutants fails to locate on the membrane because they are misfolded and trapped intracellularly by the quality control system of ER, thus exhibiting loss-of-function and causing severe obesity [90, 91]. Pharmacoperones are small hydrophobic molecules that cross the cell surface membrane and interact with the misfolded proteins within the cell. The pharmacoperones can act as molecular scaffolds and aid the misfolded proteins to native conformation, thus preventing the degradation and promoting correct trafficking to cell membrane [90, 91]. In the MC4R, previous studies reported several molecules, such as Ipsen 5i, act as pharmacoperones and successfully rescue the intracellularly retained MC4R mutants (Reviewed in [89] and [90]).

The MC4R gain-of-function mutants are also identified from obesity patients. Based on the physiological functions of MC4R, the gain-of-function MC4R mutants are expected to protect against obesity. For example, the I251L, a constitutively active MC4R mutant, is associated with constitutional lean phenotype and even the anorexia nervosa. However, from obese patients, several MC4R mutants were identified with high constitutive activities, including H76R, D146N and P230L [6, 92, 93]. Despite the unknown reasons for these mutants causing obesity, identification of the inverse agonists to these mutants shows potentially therapeutic benefits.

It has been well-established that activation of the MC4R primarily couples to the $G\alpha_s$ signaling and contributes to decreased food intake and increased energy expenditure. In addition, previous studies showed the ERK1/2 activation through MC4R is also involved in the regulation of the energy homeostasis via inhibiting food intake [60, 66]. In order to

enhance the understanding of the modulation of MC4R pharmacology by Zn^{2+} and Cu^{2+}, we investigated the ligand binding properties, and signaling properties of $G\alpha_s$ and ERK1/2 pathways of WT and mutant MC4Rs.

2.2. Materials and methods

2.2.1. Ligands, cell culture and transfection

The α-MSH was purchased from Pi Proteomics (Huntsville, AL, USA) and [Nle^4, D-Phe^7]-α-melanocyte-stimulating hormone (NDP-MSH) was purchased from Peptides International (Louisville, KY, USA). The Ipsen 5i was synthesized from Enzo Life Sciences, Inc. (Plymouth Meeting, PA, USA). Based on previous studies, the ^{125}I-NDP-MSH and ^{125}I-cAMP were iodinated by chloramine-T method for ligand binding assay and cAMP assay, respectively [94-96].

Human Embryonic Kidney (HEK) 293T cells (obtained from American Type Culture Collection, Manassas, VA, USA) were cultured for ligand binding, cAMP and western blot assays. Protocols of the N-terminal c-myc-tagged WT hMC4R subcloned into pcDNA3.1 was performed as previously described [97]. The calcium phosphate precipitation method were used for plasmids transfection [98]. Mutant hMC4Rs (H76R, D122A, C130A, D146N, P230L, F261S and C271Y) (Fig. 2.1) were previously constructed and sequenced [91, 99].

2.2.2. Ligand binding assays

The ligand binding assays were performed 48 hours after transfection. The ^{125}I-NDP-MSH was used as a tracer for competition binding assays. Cells were firstly washed two times by warm DMEM containing 1 mg/mL bovine serum albumin (referred herein as DMEM/BSA). After that, the cells were incubated at 37°C for 1 hour with the 1mL mix solution containing DMEM/BSA without or with different concentrations of α-MSH, Zn^{2+} or Cu^{2+} and 80,000 cpm of ^{125}I-NDP-MSH. The final concentration of α-MSH, Zn^{2+} or Cu^{2+} ranged from 10^{-10} to 10^{-5} M. After 1 hour's incubation, the cells were washed twice with cold Hank's balanced salt solution containing 1 mg/mL BSA to terminate the reaction and then lysed by 0.5 M NaOH for radioactive assays (Cobra II Auto-Gamma, Packard Bioscience, Frankfurt, Germany). In addition, to investigate the allosteric activity of Zn^{2+} or Cu^{2+}, ligand binding assays were conducted on WT hMC4R incubated with α-MSH (final concentrations ranging from 10^{-10} to 10^{-5} M) in the absence or presence of Zn^{2+} or Cu^{2+} (Zn^{2+}: 10^{-4}, 10^{-6}, 10^{-9} M or Cu^{2+}: 10^{-6}, 10^{-9} M).

2.2.3. Ligand stimulated cAMP production

The intracellular cAMP evaluation was performed 48 hours after transfection. The HEK293T cells transfected with WT and mutant hMC4Rs were washed twice with warm DMEM/BSA and then incubated at 37°C for 0.5 hour with warm DMEM/BSA containing 0.5 mM isobutylmethylxanthine (Sigma-Aldrich). After that, different concentrations of Zn^{2+} or Cu^{2+} were added to each well with the total volume of 1 ml. Final concentration of

Zn^{2+} and Cu^{2+} ranged from 10^{-4} to 10^{-10} M. The reaction was terminated on the ice after 1 hour incubation, and the intracellular cAMP stimulated by Zn^{2+} or Cu^{2+} was collected by adding 0.5 M percholoric acid containing 180 μg/ml theophylline (Sigma-Aldrich) and $KOH/KHCO_3$ (0.72/0.6 M). Based on the protocols described in previous study, the ^{125}I-cAMP was used to determine the intracellular cAMP levels [95]. To investigate the allosteric activity of Zn^{2+} or Cu^{2+}, cAMP assays were conducted on WT hMC4R stimulated with α-MSH (final concentrations ranging from 10^{-12} to 10^{-5} M) in the absence or presence of Zn^{2+} or Cu^{2+} (Zn^{2+}: 10^{-4}, 10^{-6}, 10^{-9} M or Cu^{2+}: 10^{-6}, 10^{-9} M).

2.2.4. Protein preparation and western blot

At 24 hours after transfection, HEK293T cells transfected with WT and mutant hMC4Rs were starved with DMEM/BSA at 37 °C for 24 hour. Approximately 24 h after starvation, HEK293T cells were treated with different concentration of Zn^{2+} or Cu^{2+} (ranged from 10^{-8} to 10^{-4} M) for 5 min at 37 °C. Based on previous study, 5 minutes' treatment was chosen for the investigation of the ERK1/2 signaling [99]. After treatment, cells were washed by ice-cold OG (150 mM NaCl and 20 mM HEPES, pH 7.4) two times and subsequently lysed with lysis buffer containing phosphatase and protease inhibitors. The total protein concentrations were determined via Bradford protein assay.

The 30 μg of protein samples were separated on 10% SDS-PAGE gel and then transferred onto PVDF membranes for immunoblotting. The PVDF membranes were blocked in the blocking buffer (10% nonfat dry milk (diluted by ddH_2O) containing 0.2%

Tween-20) for 4 hours at room temperature, and subsequently immunoblotted with rabbit anti-phosphorylated ERK1/2 (pERK1/2) antibody (Cell signaling, Beverly, MA, USA) 1:5000 and mouse anti-β-tubulin antibody (Development Studies Hybridoma Bank, University of Iowa, Iowa City, IA, USA) 1:5000 diluted in Tris-buffered saline containing Tween-20 (TBST) with 5% BSA overnight at 4 °C. On the second day, the PVDF membranes were washed by TBST for 1 hour and probed with horseradish peroxidase (HRP)-conjugated secondary antibodies, donkey anti-rabbit IgG (Jackson ImmunoResearch Laboratories, West Grove, PA, USA) 1:5000 and donkey anti-mouse IgG (Jackson ImmunoResearch Laboratories, West Grove, PA, USA) IgG 1:5000 diluted in 10% nonfat dry milk for 2 hours. The PVDF membranes were then washed with TBST three times (15 minutes once). The specific bands were detected with enhanced chemiluminescence (ECL) reagent (Thermo Scientific, Rockford, IL, USA) in the dark room and were analyzed by Image J Software (NIH, Bethesda, MD, USA) after densitometric scanning of the films.

2.2.5. Statistical analysis

The GraphPad Prism 8.0 software (San Diego, CA, USA) was used to determine the pharmacological parameters including maximal binding (B_{max}), maximal response (R_{max}), 50% maximal inhibitory concentration (IC_{50}) and 50% maximal response concentration (EC_{50}). The significance of differences in B_{max}, R_{max}, IC_{50}, EC_{50} and pERK1/2 levels between different treatments were determined by Student's t-test or one-way ANOVA followed by Tukey's multiple range test by GraphPad Prism 8.0 software.

2.3. Results

2.3.1 Ligand binding at the WT hMC4R

The hMC4R was expressed on the HEK293T cell surface and bound ^{125}I-NDP-MSH. The unlabeled endogenous agonist of α-MSH could displace ^{125}I-NDP-MSH with the IC_{50}s around 10^{-7} M (Fig. 2.2A). The Zn^{2+} and Cu^{2+} were not able to displace ^{125}I-NDP-MSH with the concentrations lower than 10^{-6} M (Figs. 2.2B and 2.2C).

2.3.2 cAMP and ERK1/2 signaling at the WT hMC4R

HEK293T cells transiently transfected with hMC4R were stimulated with different concentrations of α-MSH, Zn^{2+} and Cu^{2+}. The hMC4R exerted the dose-dependent cAMP accumulation in response to α-MSH stimulation and the R_{max} was ~20-fold higher than the basal level (Fig. 2.3A). Compared to α-MSH, we observed a much lower R_{max} (~7-fold higher than the basal level) and higher EC_{50} (~10^{-7} M) when the hMC4R was stimulated by Zn^{2+} (Fig. 2.3B). The Cu^{2+} stimulated intracellularly cAMP accumulation in a biphasic manner, with the highest cAMP level (~3-fold higher than the basal level) observed at the concentration of ~10^{-7} M (Fig. 2.3C). The HEK293T cells transiently transfected with hMC4R showed no significant difference in basal and Zn^{2+} or Cu^{2+}-stimulated pERK1/2 signaling (Fig. 2.4).

2.3.3 Allosteric property of Zn^{2+} and Cu^{2+} at the WT hMC4R

The Zn^{2+} with the concentration of 10^{-6} M failed to displace the ^{125}I-NDP-MSH but significantly stimulated the intracellular cAMP accumulation, with ~5-fold higher than the basal level (Figs. 2.5A and 2.5B). The Zn^{2+} with the concentrations of 10^{-9}, 10^{-6} and 10^{-4} M resulted in a leftward-shift of the α-MSH-induced dose-dependent ligand binding competitive curve with significantly decreased IC_{50}s (Fig. 2.5C, Table 2.1), and a rightward-shift of the α-MSH-induced dose-response cAMP accumulation curve with significantly decreased R_{max}s (Fig. 2.5D, Table 2.2).

Likewise, the Cu^{2+} with the concentration of 10^{-6} M cannot displace the ^{125}I-NDP-MSH but can weakly stimulate the intracellular cAMP accumulation (Figs 2.6A and 2.6B). Lower concentration of Cu^{2+} (~10^{-9} M) caused a leftward-shift of the α-MSH-induced dose-dependent ligand binding competitive curve and cAMP accumulation curve with significantly decreased IC_{50} and EC_{50} (Figs. 2.6C and 2.6D, Tables 2.3 and 2.4). The Cu^{2+} with the concentration of 10^{-6} M contributed to a rightward-shift of the α-MSH-induced ligand binding competitive curve and the α-MSH-induced cAMP accumulation curve with significantly increased IC_{50} and EC_{50} (Figs. 2.6C and 2.6D, Tables 2.3 and 2.4).

2.3.4 cAMP signaling at MC4R mutants (variants)

(1) Gain-of-function mutants

Several naturally occurring *MC4R* mutations have been identified in obese patients and these mutants exhibit constitutive activation in $G\alpha_s$ signaling (Figs. 2.1 and 2.7A). The three mutant (H76R, D146N and P230L) hMC4Rs exerted the dose-dependent cAMP accumulation in response to Zn^{2+} stimulation (Fig. 2.7B). Consistent to the WT hMC4R, mutants of H76R, D146N and P230L displayed biphasic manners in cAMP production in response to Cu^{2+} stimulation (Fig. 2.7C).

(2) Loss-of-function Mutants

RM493 (setmelanotide) is the second-generation MC4R agonist with therapeutic benefits to obesity patients [100]. We observed that the Zn^{2+} and Cu^{2+} exhibited no effects on intracellular cAMP accumulation at WT hMC4R stimulated by RM493 (Fig. 2.8A). The F261S and C271Y are two naturally occurring loss-of-function *MC4R* mutations which are identified from obese patients. Compared to the WT hMC4R, mutants of F261S and C271Y were less capable of activating cAMP producing (Fig. 2.8B). With 10^{-6} M Ipsen5i (pharmacoperone) treatment, the mutants of F261S and C271Y exerted similar maximal cAMP accumulation in response to RM493 stimulation when compared to WT hMC4R (Fig. 2.8C). With the physiologically relevant concentration, Zn^{2+} and Cu^{2+} showed no effects on RM493-stimulated intracellular cAMP accumulation at mutant hMC4R of F261S (Fig. 2.8D).

(3) WT-like Mutants (Variants)

With the recently reported MC4R crystal structure in 2020, Cone *et al.* showed the metal ions coordinated with three negatively charged residues of E100, D122 and D126 at MC4R [101]. D122A, a “WT-like” variant, showed normal α-MSH-stimulated cAMP producing but were less capable of activating cAMP producing in response to Zn^{2+} stimulation (Fig. 2.9A). Another “WT-like” hMC4R variant, C130A, exerted no significant difference in cAMP production in response to Zn^{2+} or Cu^{2+} stimulation (Fig. 2.9B).

2.4. Discussion

Historically, Pert, Pasternak and their colleagues firstly discovered the ligands binding of opioid receptors are regulated by metal ions [102-104]. After that, hundreds of studies confirmed metal ions either directly act as the orthosteric ligands (such as calcium (Ca^{2+}) and calcium-sensing receptor (CaSR) [105]), or allosterically modulates the GPCRs (Reviewed in [1, 70, 106]). We showed the Zn^{2+} and Cu^{2+} could not displace the ^{125}I-NDP-MSH (Fig. 2.2). Because of the lack of radiolabeled Zn^{2+} and Cu^{2+}, we were unable to investigate the binding of Zn^{2+} and Cu^{2+} by direct binding assay. However, based on functional effects of Zn^{2+} and Cu^{2+} (Figs. 2.3, 2.5 and 2.6), we proposed that Zn^{2+} and Cu^{2+} could bind to hMC4R at distinct site(s) from α-MSH (orthosteric ligand) binding sites. Based on our studies, we showed the Zn^{2+} and Cu^{2+} exerted allosteric agonism and modulation in cAMP signaling at hMC4R (Figs. 2.3, 2.5 and 2.6). We also observed that Zn^{2+} and Cu^{2+} induced biased signaling at hMC4R, as they selectively activated the canonical cAMP signaling, but exerted no activation in pERK1/2 signaling (Figs. 2.3 and 2.4).

In mouse MC1R, studies showed that, in the absence of the α-MSH, Zn^{2+} is envisioned to bind between C271 located in the extracellular loop 3 (ECL3) and the D119 located in the transmembrane domain III (TM-III) [74, 76]. Because the α-MSH itself (Arg of α-MSH) binds to D119 with high affinity, with the presence of the α-MSH, Zn^{2+} interacts with His residue of the α-MSH and the free C271 of MC1R, thus allosterically modulating the potency of the α-MSH [76]. We observed conserved Zn^{2+} binding motifs in TM-III and ECL3 between MC1R and MC4R (Fig. 2.1). Despite Zn^{2+} failing to displace ^{125}I-NDP-MSH, it acted as an allosteric ligand at WT hMC4R with weak agonism and strong allostery (Figs. 2.2, 2.3 and 2.5). The Zn^{2+} significantly enhanced the binding affinity but decreased the potency of α-MSH, with reduced the IC_{50}s and R_{max}s (Fig. 2.5, Tables 2.1 and 2.2). Consistently, previous studies revealed that Zn^{2+} serves as allosteric modulator at MC1R, G protein-coupled dopamine receptors, serotonin receptor (5-HT_{1A} receptor) and adrenergic receptor (α_{1A}-AR and β_2-AR) [74, 76, 107-109].

Compared to Zn^{2+}, the allosteric property of Cu^{2+} was much complicated. At hMC4R, Cu^{2+} acted as an allosteric enhancer and resulted in reduced IC_{50} and EC_{50} of α-MSH in a lower concentration (~10^{-9} M, Fig. 2.6, Tables 2.3 and 2.4). However, Cu^{2+} behaved as an allosteric inhibitor in a high concentration around 10^{-6} M and significantly enhanced the IC_{50} and EC_{50} of α-MSH (Fig. 2.6, Tables 2.3 and 2.4). Link *et al.* recently published a paper in 2019 and showed Cu^{2+} exhibits a biphasic effect on NDP-MSH-induced intracellularly cAMP accumulation at MC4R [82]. Likewise, the biphasic effect on divalent cation-regulated allostery was also observed in other GPCRs including rhodopsin, β_2-AR

and 5-HT_{1A} receptor [107-111]. For example, at 5-HT_{1A} receptor, the divalent cation allosterically enhances the agonist binding affinity with lower concentrations (10 μM) but decreases the agonist binding affinity in high concentrations (500 μM) [109]. The divalent metal ions show high affinity to the aromatic nitrogen of histidine and carboxy group of aspartate and glutamate [112-114]. A great number of studies revealed that the metal ions exert different physiology and pharmacology via binding to GPCRs with distinct site(s) [106-111]. Although studies on the crystal structure of the Cu^{2+}-bound hMC4R are limited, a recent study showed the divalent metal ion of Ca^{2+} binds to E100 (TM-II), D122 (TM-III) and D126 (TM-III) at hMC4R [101]. We also observed several potential metal ion binding sites that are located at extracellular domains, including E29, D37, E42, E111, E113 and C130. Based on these evidences, we might propose that Cu^{2+} coordinates with different binding pockets at hMC4R, thereby exhibiting biphasic allostery.

At WT hMC4R, the Cu^{2+} stimulated cAMP producing in a biphasic manner (Fig. 2.3). Likewise, previous studies reported the physiologically relevant Cu^{2+} concentrations could inhibit the basal activity of hMC4R [82]. We observed that Cu^{2+} exhibited biphasic manner in modulating cAMP accumulation at constitutively active mutant hMC4Rs identified from obesity patients (Fig. 2.7). Considering the evidence that the highest copper concentrations in brain are ~70 μM [77], our results suggested that Cu^{2+} could probably exert as an inverse agonist and decrease the constitutive activities at mutant hMC4Rs, thus showing therapeutic benefits in the development of the anti-obesity drugs.

The clinical data showed the second-generation MC4R agonist, RM493, contributes

to a reduction in hyperphagia and body weight without notable side effects in cardiovascular functions [100]. We observed that Zn^{2+} and Cu^{2+} exhibited no effects on RM493-stimulated cAMP accumulation at WT hMC4R (Fig. 2.8), which is consistent with previous studies in MCRs structures. The central amino acid motif (His-Phe-Arg-Trp) of α-MSH or RM493 is involved in ligand recognition and ligand-induced signaling at hMC4R [115]. The Zn^{2+} exerts allosteric effects by coordinating with His residue of the α-MSH [74, 76]. The His residue of the α-MSH coordinates with hMC4R at Y268 and S191, while the His residue of RM493 coordinates with hMC4R at N123 and F184 [100]. The different binding pockets of α-MSH and RM493 at hMC4R probably resulted in different allosteric effects of Zn^{2+} and Cu^{2+}. The Zn^{2+} and Cu^{2+} also showed no influences on RM493-stimulated cAMP producing at rescued MC4R mutant of F261S (Fig. 2.8), probably indicating that, with the physiologically relevant concentrations, therapeutic effects of RM493 would be not attenuated by endogenous Zn^{2+} and Cu^{2+}.

Our previous studies showed the D122A is a “WT-like” variant with similar cell surface expression and R_{max} in response to NDP-MSH stimulation when compared to WT hMC4R [94]. Based on recently identified MC4R crystal structure, D122 is one of the three negatively charged residues (D122, E100,and D126) at MC4R that interact with Ca^{2+} [101]. We observed that, compared to WT, the D122A exerted significantly decreased Zn^{2+}-induced cAMP producing (Fig. 2.9), suggesting D122 is a potential binding site of Zn^{2+} at MC4R.

2.5 Conclusion

In this study, we showed Zn^{2+} and Cu^{2+} acted as biased allosteric modulators at hMC4R. The Zn^{2+} and Cu^{2+} selectively modulate the cAMP signaling but not the ERK1/2 signaling. Notably, the biphasic cAMP accumulation induced by Cu^{2+} was observed not only at WT but also at obesity-associated mutant MC4Rs with high constitutive activities, suggesting this biphasic action might contribute to novel therapeutic opportunities for obese treatment. The Zn^{2+} acted as an allosteric modulator at WT hMC4R, enhancing the binding affinity but decreasing the potency (R_{max}) of α-MSH. Cu^{2+} acted as an allosteric enhancer in a lower concentration (~10^{-9} M), but an allosteric inhibitor in a high concentration around 10^{-6} M. The Zn^{2+} and Cu^{2+} failed to impact the RM493-induced cAMP accumulation probably because RM493 exerts distinct binding site with α-MSH at hMC4R. The D122, one of the three binding sites of calcium, also acted as a potential binding site of Zn^{2+}. Our study might provide new opportunities for the development of the drugs with improved profile by coordinating with metal ions.

Table 2.1 Allosteric effects of Zn^{2+} on ligand binding at WT hMC4R.

	α-MSH + Vehicle	α-MSH + Zn^{2+} (10^{-9} M)	α-MSH + Vehicle	α-MSH + Zn^{2+} (10^{-6} M)	α-MSH + Vehicle	α-MSH + Zn^{2+} (10^{-4} M)
B_{max} (%)	100	97.15	100	111.13	100	99.10
IC_{50} (nM)	172.08 ± 39.34	9.96 ± 1.17*	223.20 ± 29.22	4.77 ± 1.07*	165.50 ± 30.57	1.43 ± 0.23*

Asterisk (*) indicates significantly different from the the parameter of vehicle control ($P < 0.05$).

Table 2.2 Allosteric effects of Zn^{2+} on α-MSH-stimulated cAMP siganling at WT hMC4R.

	α-MSH + Vehicle	α-MSH + Zn^{2+} (10^{-9} M)	α-MSH + Vehicle	α-MSH + Zn^{2+} (10^{-6} M)	α-MSH + Vehicle	α-MSH + Zn^{2+} (10^{-4} M)
R_{max} (%)	100	76.18*	100	55.49*	100	47.32*
EC_{50} (nM)	0.17 ± 0.02	0.78 ± 0.13*	0.17 ± 0.02	0.27 ± 0.15	0.17 ± 0.02	0.15 ± 0.00

Asterisk (*) indicates significantly different from the the parameter of vehicle control ($P < 0.05$).

Table 2.3 Allosteric effects of Cu^{2+} on ligand binding at WT hMC4R.

	α-MSH + Vehicle	α-MSH + Cu^{2+} (10^{-9} M)	α-MSH + Vehicle	α-MSH + Cu^{2+} (10^{-6} M)
B_{max} (%)	100	88.41	100	94.40
IC_{50} (nM)	127.37 ± 7.20	32.25 ± 15.37*	127.37 ± 7.20	431.07 ± 11.27*

Asterisk (*) indicates significantly different from the the parameter of vehicle control ($P < 0.05$).

Table 2.4 Allosteric effects of Cu^{2+} on α-MSH-stimulated cAMP siganling at WT hMC4R.

	α-MSH + Vehicle	α-MSH + Cu^{2+} (10^{-9} M)	α-MSH + Vehicle	a-MSH + Cu^{2+} (10^{-6} M)
R_{max} (%)	100	131.74	100	80.11
EC_{50} (nM)	0.34 ± 0.05	0.03 ± 0.01*	0.12 ± 0.00	1.25 ± 0.19*

Asterisk (*) indicates significantly different from the the parameter of vehicle control ($P < 0.05$).

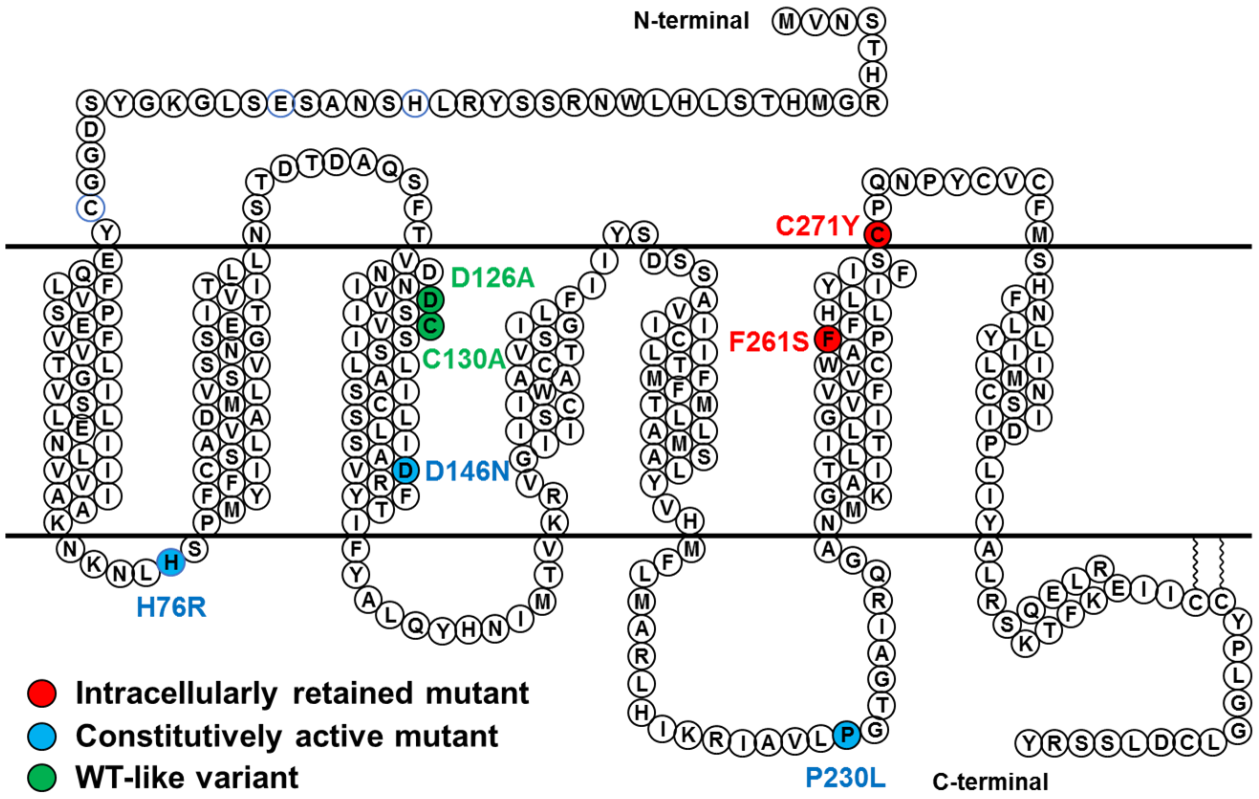

Fig. 2.1. Schematic model of hMC4R.

The hMC4R mutants and variants in this study are highlighted with red filling (naturally occurring intracellularly retained mutants identified from obesity patients), blue filling (naturally occurring constitutively active mutations identified from obesity patients) and green filling (WT-like variant obtained from site-direct mutagenesis).

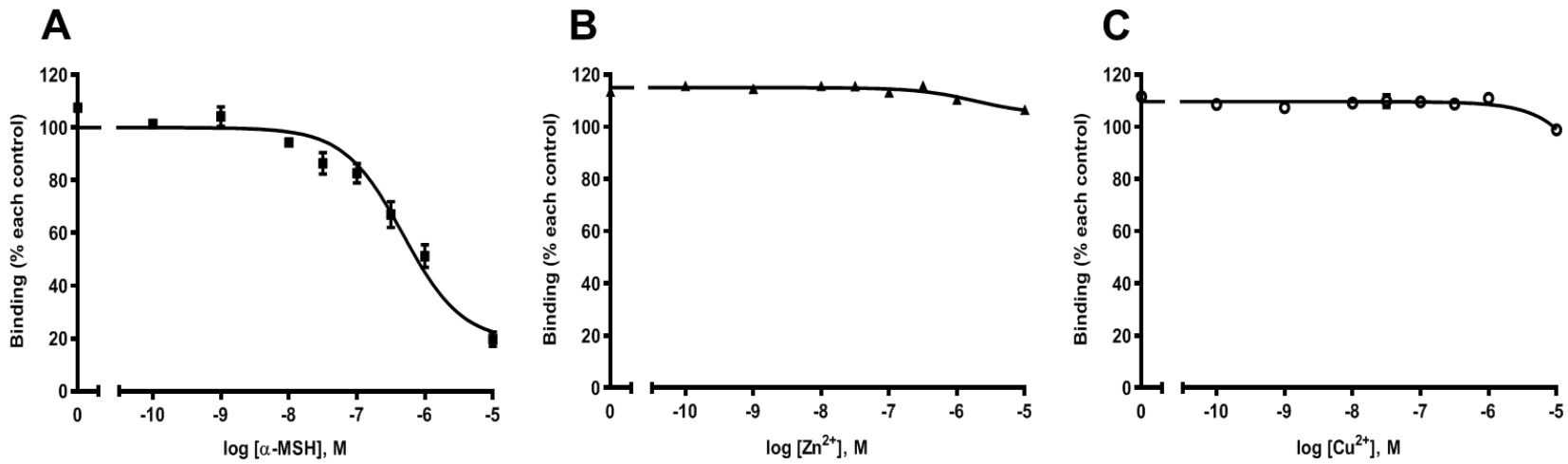

Fig. 2.2. Ligand binding properties of the hMC4R with α-MSH (A), Zn^{2+} (B) or Cu^{2+} (C) as the competitor.

Binding at HEK293T cells transiently transfected with WT hMC4R were measured by displacement of ^{125}I-NDP-MSH with different concentrations of unlabeled α-MSH (A), Zn^{2+} (B) or Cu^{2+} (C). Results are expressed as percent of WT maximal binding ± range from duplicate determinations within one experiment. The curves are representative of 3 independent experiments. All experiments were performed at least three times with similar results.

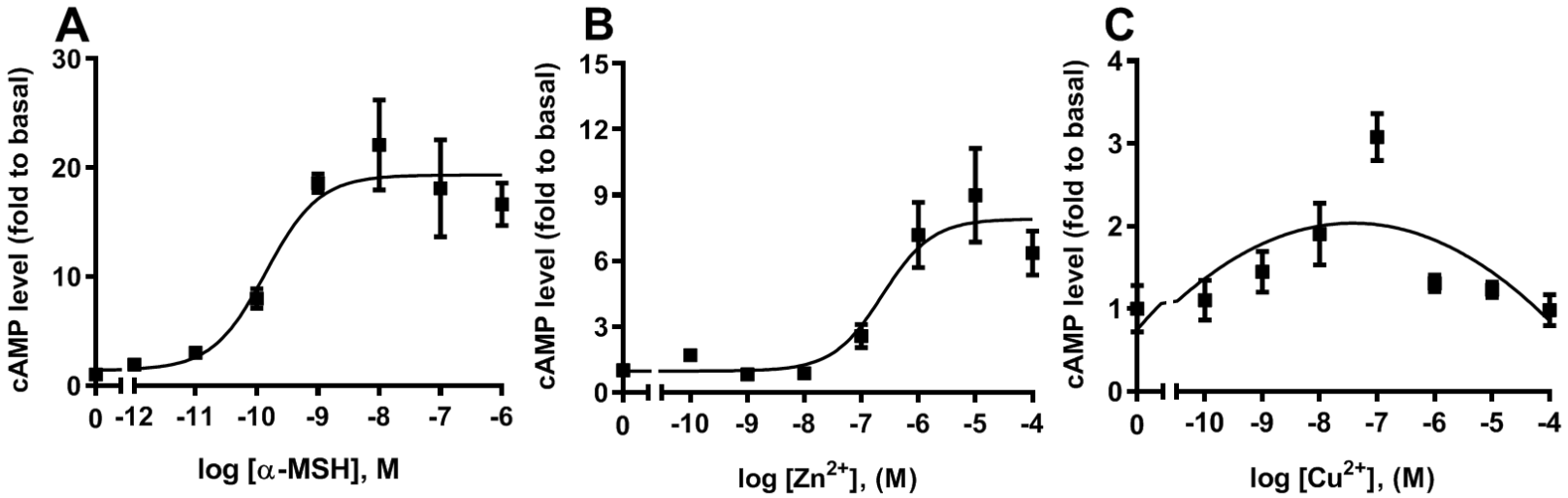

Fig. 2.3. The cAMP signaling properties of the hMC4R stimulated by different concentrations of α-MSH (A), Zn^{2+} (B) or Cu^{2+} (C).

Results shown are expressed as fold to basal level ± range from triplicate determinations within one experiment. The curves are representative of 3 independent experiments. All experiments were performed at least three times with similar results.

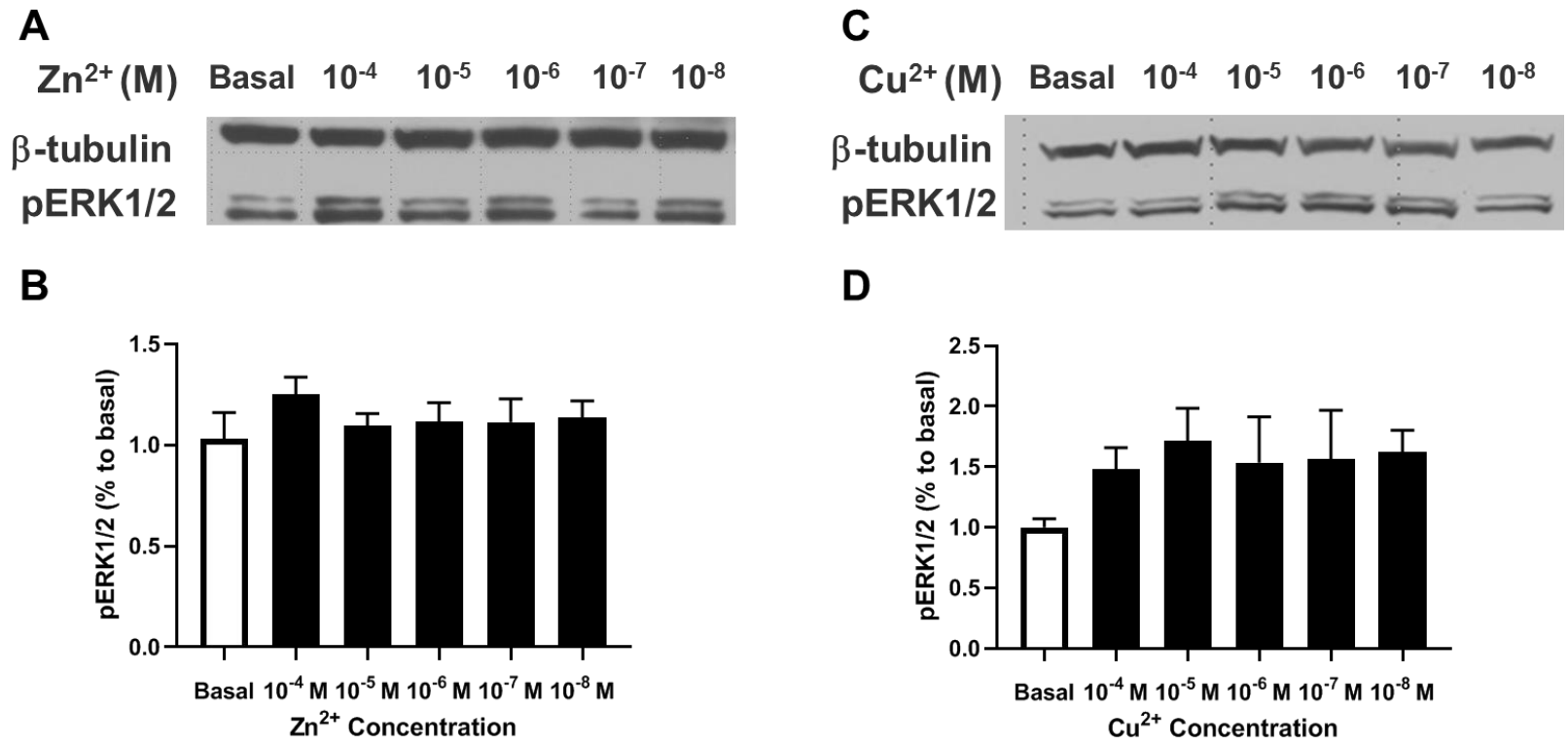

Fig. 2.4. The ERK1/2 signaling properties of the hMC4R initiated by Zn^{2+} (A, B) or Cu^{2+} (C, D).

Panel A or C shows the representative image of one experiment. Panel B or D shows the densitometry results of ERK1/2 phosphorylation. Results are expressed as the percentage of the value obtained in non-stimulated HEK293T cells transiently transfected with WT hMC4R. All experiments were performed at least three times with similar results.

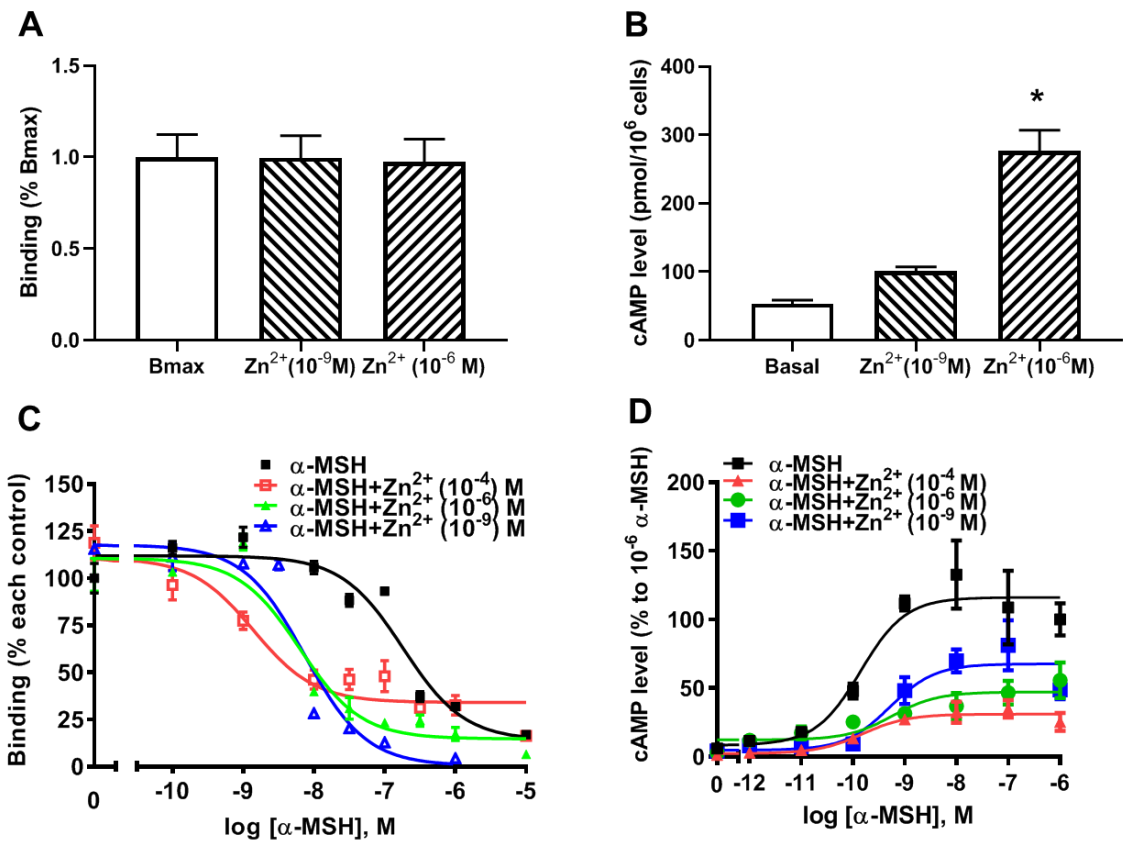

Fig. 2.5. Effects of Zn^{2+} on liangd binding (A, C) and cAMP signaling (B, D) properties of the hMC4R.

The Zn^{2+} with the concentration of 10^{-6} or 10^{-9} M failed to displace the ^{125}I-NDP-MSH (A) while enhcanced the intracellular cAMP accumualtiom (B). The Zn^{2+} with the concentration of 10^{-4}, 10^{-6} or 10^{-9} M allostrically modulted the binding affinity (C) and the potency of α-MSH (D). Results shown are from duplicate (A, C) or triplicate (B, D) determinations within one experiment. The curves are representative of 3 independent experiments. All experiments were performed at least three

times with similar results. Asterisk (*) indicates significantly different to basal cAMP level ($P < 0.05$).

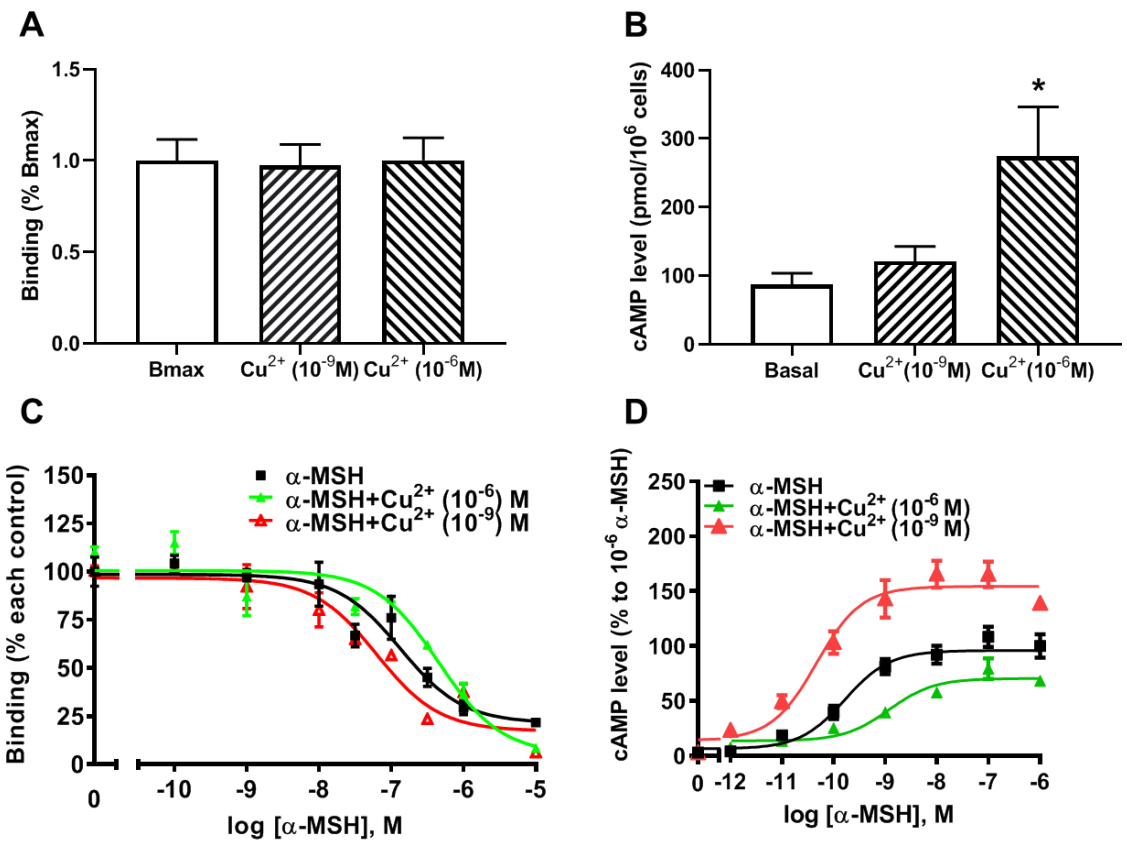

Fig. 2.6. Effects of Cu^{2+} on liangd binding (A, C) and cAMP signaling (B, D) properties of the hMC4R.

The Cu^{2+} with the concentration of 10^{-6} or 10^{-9} M failed to displace the ^{125}I-NDP-MSH (A) while enhcanced the intracellular cAMP accumualtiom (B). The Cu^{2+} with the concentration of 10^{-6} or 10^{-9} M allostrically modulted the binding affinity (C) and the potency of α-MSH (D). Results shown are from duplicate (A, C) or triplicate (B, D) determinations within one experiment. The curves are representative of 3 independent experiments. All experiments were performed at least three times with

similar results. Asterisk (*) indicates significantly different to basal cAMP level ($P < 0.05$).

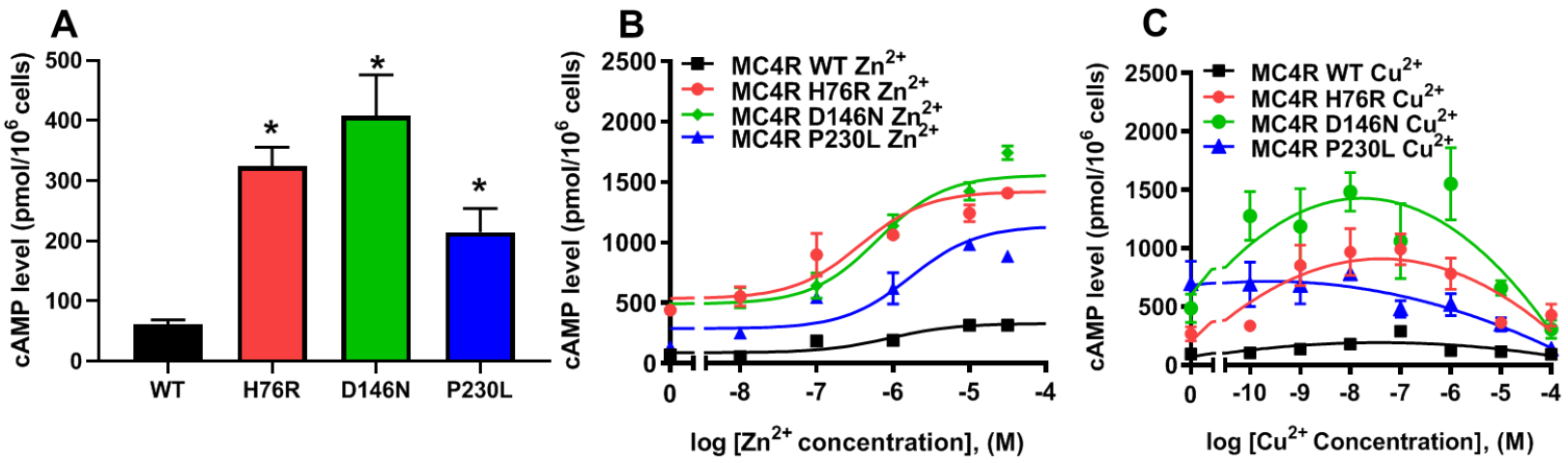

Fig. 2.7. The cAMP signaling properties of the gain-of-function hMC4R mutants stimulated by different concentrations of Zn^{2+} or Cu^{2+}.

The basal cAMP activities (A), the cAMP levels stimulated by Zn^{2+} (B) or stimulated by Cu^{2+} (C). Results shown are from triplicate determinations within one experiment. The curves are representative of 3 independent experiments. All experiments were performed at least three times with similar results. Asterisk (*) indicates significantly different to WT basal cAMP level ($P < 0.05$).

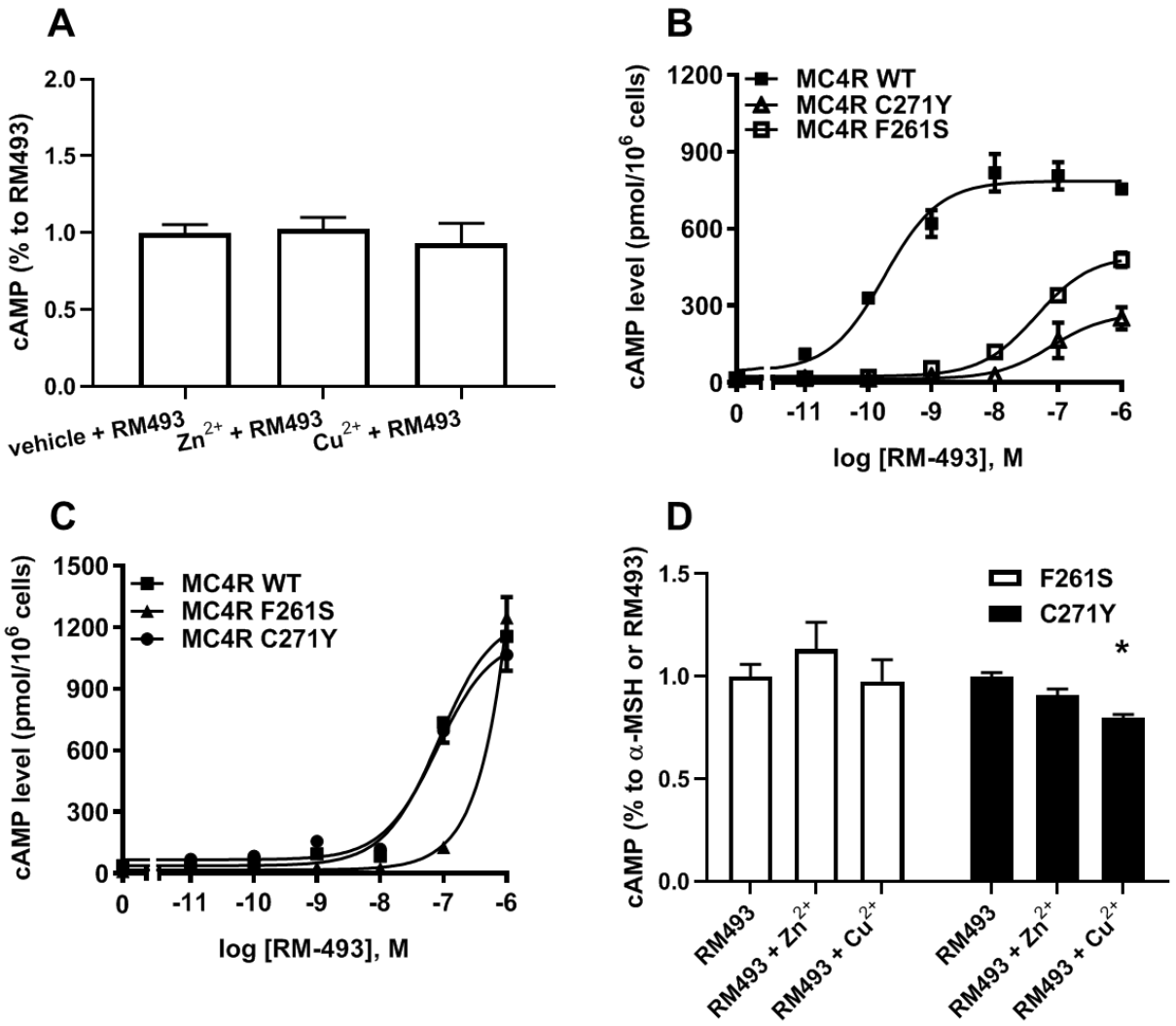
A
cAMP (% to RM493)
2.0
1.5
1.0
0.5
0.0
vehicle + RM493
Zn2+ + RM493
Cu2+ + RM493
B
cAMP level (pmol/10^6 cells)
MC4R WT
MC4R C271Y
MC4R F261S
1200
900
600
300
0
0
-11
-10
-9
-8
-7
-6
log [RM-493], M
C
cAMP level (pmol/10^6 cells)
MC4R WT
MC4R F261S
MC4R C271Y
1500
1200
900
600
300
0
0
-11
-10
-9
-8
-7
-6
log [RM-493], M
D
cAMP (% to α-MSH or RM493)
F261S
C271Y
*
1.5
1.0
0.5
0.0
RM493
RM493 + Zn2+
RM493 + Cu2+
RM493
RM493 + Zn2+
RM493 + Cu2+

Fig. 2.8. The cAMP signaling properties of the WT (A) or loss-of-function mutant hMC4Rs (B, C and D) stimulated by α-MSH or different concentrations of RM493 (without Ipsen 5i (B), with Ipsen 5i (C and D)).

Results shown are from triplicate determinations within one experiment. The curves are representative of 3 independent experiments. All experiments were performed at least three times with similar results. In figure A, the final concentrations of RM493, Zn^{2+} and Cu^{2+} are 10^{-6}, 10^{-5} and 10^{-7} M, respectively. In figure D, the final concentration of RM493, Zn^{2+} and Cu^{2+} is 10^{-6} M, respectively. Asterisk (*) indicates significantly different to vehicle ($P < 0.05$).

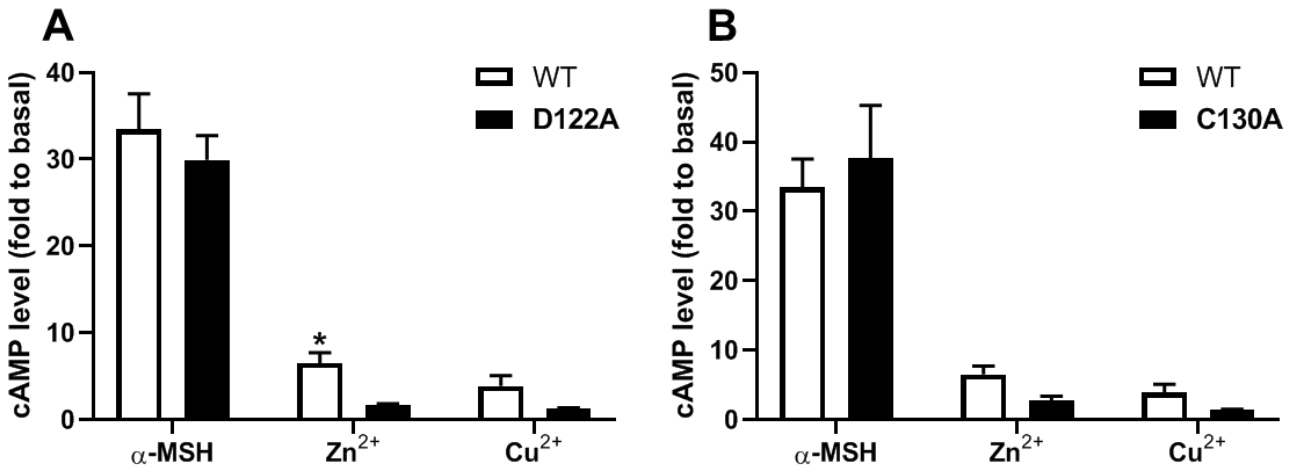

Fig. 2.9. The cAMP signaling properties of the WT or "WT-like" mutant hMC4Rs stimulated by α-MSH, Zn^{2+} and Cu^{2+}. Results shown are from triplicate determinations within one experiment. All experiments were performed at least three times with similar results. The final concentrations of α-MSH, Zn^{2+} and Cu^{2+} are 10^{-7}, 10^{-5} and 10^{-7} M, respectively. Asterisk (*) indicates significantly different to WT cAMP level ($P < 0.05$).

Chapter 3: Melanocortin-4 receptor in spotted sea bass, *Lateolabrax maculatus*: cloning, tissue distribution, physiology, and pharmacology

3.1. Introduction

Melanocortin peptides are posttranslational products of proopiomelanocortin (POMC) that include α-, β-, and γ- melanocyte-stimulating hormones (α-, β-, and γ-MSH) and adrenocorticotropic hormone (ACTH) (reviewed in [14, 15]). Melanocortin peptides exert their effects by activating melanocortin receptors (MCRs). Five MCRs have been cloned, named MC1R to MC5R based on the order in which they were first cloned (reviewed in [7, 116]). MC4R belongs to Family A rhodopsin-like G protein-coupled receptors (GPCRs) and it primarily couples to the stimulatory G protein (G_s) to activate adenylyl cyclase, leading to increased level of intracellular cyclic adenosine monophosphate (cAMP) to activate downstream protein kinase A (PKA). α-MSH, ACTH and other POMC-derived peptides are endogenous agonists and Agouti-related peptide (AgRP) is endogenous antagonist of MC4R. In addition, analogs of α-MSH and some small molecules have also been identified as MC4R ligands. [Nle4, D-Phe7]-α-MSH (NDP-MSH) is a superpotent analog of α-MSH that is widely used in pharmacological studies of MCRs [117]. THIQ, (N-[(3R)-1,2,3,4-tetrahydroisoquinolinium-3-ylcarbonyl]-(1R)-1-(4-chlorobenzyl)-2-[4-cyclohexyl-4-(1H-1,2,4-triazol-1-ylmethyl)piperidin-1-yl]-2-oxoethylamine), is a small molecule agonist [118].

Activation of neurons expressing neuropeptide-Y (NPY) and AgRP increase food

intake, while activation of neurons expressing POMC decrease food intake in human and mice (reviewed in [6]). POMC-derived peptides, such as α-MSH and ACTH, are anorexigenic by activating MC4R. In human, two groups independently reported that *MC4R* frameshift mutations are associated with severe early-onset obesity in 1998 [39, 40]. Since then, a total of at least 175 distinct *MC4R* mutations have been identified from patients associated with obesity and other diseases (reviewed in [119, 120]). Mice lacking *Mc4r* expression have increased food intake and decreased energy expenditure, resulting in obesity and hyperinsulinemia [35]. In addition to regulation of energy balance, recent studies reported that MC4R is also involved in reproductive functions via regulating hypothalamus-pituitary-gonad axis and prolactin secretion [121-123].

MC4R and other MCRs have also been identified in tetrapods and teleosts. In tetrapods, all MCRs (MC1R-MC5R) have been identified and higher MC4R expression was observed in central nervous system [7, 124]. In teleosts, MC4R is expressed in both central and peripheral tissues [125-131]. In cavefish (*Astyanax mexicanus*), nonsynonymous *mc4r* mutations cause increased appetite and starvation resistance [132]. In zebrafish, overexpression of AgRP leads to obesity phenotype [133]. Intracerebroventricular (i.c.v) injection of MC4R agonist decreases food intake, while injection of MC4R antagonist increases food intake in goldfish and rainbow trout (*Oncorhynchus mykiss*) [134, 135]. These results suggest that teleost MC4R also acts as the regulator in energy balance. Teleost MC4Rs are also associated with the onset of puberty, growth and body size, and sexual behaviors in a species-specific manner in different teleosts [136, 137]. We showed that administration of MC4R ligands to spotted

scat can change expression of genes related to reproduction [138].

Our previous studies showed that teleost MC4Rs have different pharmacological characteristics from mammalian MC4Rs. For example, compared to human MC4R (hMC4R), teleost MC4Rs display high basal activities [128-131]. Moreover, THIQ acts as an orthosteric agonist to activate mammalian MC4Rs; however, it activates teleost MC4Rs allosterically [128, 130]. Therefore, in the present study, we used spotted sea bass, *Lateolabrax maculatus*, as an animal model to systematically investigate *Lm*MC4R physiology and pharmacology. We investigated mRNA expression and localization of *mc4r* in different tissues and changes in expression after fasting challenge. We also performed detailed pharmacological studies on *Lm*MC4R including ligand binding and signaling. We included hMC4R in these experiments for comparison.

3.2. Materials and methods

3.2.1. Gene cloning and sequence alignment

All procedures involving fish followed the guidelines and were approved by the Animal Research and Ethics Committee of Ocean University of China (Permit Number: 20141201).

Total RNA was extracted from spotted sea bass brain using TRIzol (Invitrogen, Carlsbad, CA, USA). The concentration and integrity of total RNA were evaluated by the

Agilent 2100 Bioanalyzer system (Agilent Technologies, Santa Clara, CA, USA). One microgram of RNA was used to synthesize first-strand cDNA using random primers and reverse transcriptase M-MLV with gDNA Eraser (TaKaRa, Japan). To amplify cDNA fragments of *mc4r*, PCR was performed and primers of *mc4r* were designed based on transcriptome databases (Table 3.1). PCRs were performed in a 25 μl mixture containing 1 μl cDNA, 0.5 μl of each primer, 2 μl dNTPs, 2.5 μl 10×PCR buffer, 18.25 μl ddH_2O, and 0.25 μl Taq DNA Polymerase (TaKaRa) with following program: initial denaturation at 94 °C for 5 min, followed by 40 cycles at 94 °C for 30 s, 60 °C for 30 s and 72 °C for 1 min. The reaction was terminated with a further extension of 5 min at 72 °C. The amplification products were separated by 1.5% w/v agarose gel stained with ethidium bromide. Target fragment was purified by TIANgel Midi Purification kit (Tiangen, Beijing, China), and then subcloned into Trans1-T1 *Escherichia coli* (TransGen Biotech, Beijing, China). Two positive clones were sequenced on an ABI 3700 sequencer (Applied Biosystems, Foster City, CA, USA).

Multiple alignments of amino acid sequences of MC4Rs in different species were performed with DNAMAN 6.0 (Lynnon Biosoft, San Ramon, CA, USA). The percentage of similarity between amino acid sequences were calculated with DNAMAN 6.0. Phylogenetic tree based on amino acid sequences was constructed by Neighbor-joining and Maximum likelihood methods with Mega 6.0 software. The strength of branch relationships was assessed by bootstrap replication (N 1/4 1,000 replicates).

3.2.2. Tissue distribution of *mc4r*

Total RNA was extracted from fresh tissues (pituitary, brain, liver, kidney, spleen, intestine, muscle, gonads, gill, heart) and treated with RNase-free DNase I (Thermo Scientific Corp, Waltham, MA, USA). M-MLV Reverse Transcriptase (Promega, Madison, WI, USA) was used for cDNA synthesis with oligo-dT (12-18) primers. The cDNA was subsequently used for amplification using specific primers based on *mc4r* sequence from transcriptome database. The quantitative reverse transcription PCR (qRT-PCR) reaction consisted of a total volume of 20 μl mixture containing 10 μl SYBR®FAST qPCR Master Mix (2X), 0.4 μl ROX reference dye, 2 μl template cDNA, 0.4 μl of each primer and 6.8 μl of nuclease-free water. PCR amplification was in a 96-well optical plate at 95 °C for 5 s, followed by 40 cycles of 95 °C for 5 s, 60 °C for 30 s, and finally followed by a dissociation curve to verify the specificity of amplified products. qRT-PCR was performed using the StepOne Plus Real-Time PCR system (Applied Biosystems) and the $2^{-\Delta\Delta CT}$ method was used to analyze the relative expression [139].

3.2.3. Localization of *mc4r* in brain, liver, and pituitary

Brain, liver, and pituitary samples were fixed in buffered 4% paraformaldehyde for 24 h and then dehydrated with a graded series of ethanol solution (70 - 100%), cleared in xylene and embedded in paraffin. Seven-micron sections were cut for *in situ* hybridization. The primers for *in situ* hybridization of *mc4r* was listed in Table 3.1. Sense and antisense digoxigenin- (DIG)- labeled riboprobes were synthesized from the sequence (574bp-

1232bp) of the *mc4r* using DIG RNA Labeling Kit (Roche Diagnostics, Mannheim, Germany). DIG *in situ* hybridization was performed as described previously [140]. Briefly, the sections were rehydrated by a graded series of ethanol solution (100 - 70%) and then permeabilized with 0.1 M HCl for 8 min, followed by proteinase K (20 ng/μl) treatment for 20 min, prehybridized at 42 °C for 1 hour, and hybridized with DIG-labeled riboprobes (500 μg/ml) at 58 °C overnight. After hybridization, the sections were washed and blocked with blocking reagent (Roche Diagnostics). DIG was detected with an alkaline phosphatase-conjugated anti-DIG antibody (Roche Diagnostics; diluted 1:1000) and chromogenic development was conducted with NBT/BCIP (Roche Diagnostics). The samples were dehydrated by a series of graded ethanol, cleared in xylene, sealed with neutral resin and taken with a microscope (Olympus, Japan).

3.2.4. Physiological functions: Fasting challenge

Approximately 40 basses per group (for short term fasting challenge, 100.00 ± 12.32 g) and 120 fish per group (for long term fasting challenge, 5.88 ± 0.26 g) were acclimatized in the aquaria at 25.2 °C for at least one week. In short-term fasting, six basses per group (three duplicated groups were set) were sampled at 0, 1, 6, 12 and 24 h post fasting. In long-term fasting, 120 individuals of spotted sea bass were randomly divided into six 120-liter-rectangular containers. Three to six fish per container were sampled after 8-week's fasting. All sampled fish were treated with eugenol and sampled immediately. Brain tissues were collected and temporarily placed into liquid nitrogen and finally stored at -80 °C for mRNA extraction.

3.2.5. Pharmacological characterization

(1) Ligands, cell culture and transfection

NPD-MSH, α-MSH, ACTH (1-24), and THIQ were used. NDP-MSH from Peptides International (Louisville, KY, USA), α-MSH from Pi Proteomics (Huntsville, AL, USA), ACTH (1–24) from Phoenix Pharmaceuticals (Burlingame, CA, USA), THIQ from Tocris Bioscience (Ellisville, MO, USA). ^{125}I-NDP-MSH was iodinated as previously described [94] and ^{125}I-cAMP was iodinated in our lab via chloramine T method [95, 96].

The N-terminal c-myc-tagged wild-type hMC4R subcloned into pcDNA3.1 was described previously [97]. Open reading frame (ORF) of *Lm*MC4R was identified by transcriptome data and the N-terminal c-myc-tagged ORF of *Lm*MC4R was then subcloned into pcDNA3.1 vector by GenScript (Piscataway, NJ, USA) to obtain the plasmid expressing *Lm*MC4R.

Three peptide ligands (α-MSH, ACTH (1-24) and NDP-MSH) and one small molecule ligand (THIQ) were used to evaluate ligand binding and signaling properties of *Lm*MC4R. α-MSH and ACTH are endogenous agonists of all MCRs with the exception that α-MSH cannot activate MC2R. In this study, ACTH (1-24) instead of full-length ACTH (1-39) was used to investigate the pharmacological characteristics of *Lm*MC4R as the first 24 amino acids of ACTH are highly conversed in different species ranging from human to teleosts

and ACTH (1-24) is equipotent to the full-length ACTH [141, 142]. THIQ is small molecule ligand of hMC4R and our previous studies revealed that they act as pharmacological chaperones, rescuing intracellularly retained hMC4R mutants [6, 89, 91, 143, 144].

Human Embryonic Kidney (HEK) 293T cells (Manassas, VA, USA) were cultured and used for pharmacological assays. Plasmid transfection was performed as described before [98]. At 48 h after transfection, binding and signaling assays were performed.

(2) Cell surface and total expressions of hMC4R and *Lm*MC4R

HEK293T cells were transiently transfected with hMC4R or *Lm*MC4R plasmid with N-terminal c-myc tag. Forty-eight hours after transfection, cells were incubated with mouse anti-myc 9E10 monoclonal antibody (Developmental Studies Hybridoma Bank, The University of Iowa, Iowa City, IA, USA) diluted 1:40 for 1 h. Cells were then washed and incubated with Alexa Fluor 488-labeled goat anti-mouse antibody (Invitrogen, Grand Island, NY, USA) diluted 1:2000 for 1 h. The C6 Accuri Cytometer (Accuri Cytometers, Ann Arbor, MI, USA) was used for analysis. Fluorescence of cells expressing the empty vector (pcDNA3.1) was used for background staining. The expression of the *Lm*MC4R was calculated as percentage of hMC4R expression using the following formula: [(*Lm*MC4R − pcDNA3.1)/(hMC4R − pcDNA3.1) × 100%] [145].

(3) Ligand binding assays

For ligand binding, 48 h after transfection, cells were washed twice with warm DMEM containing 1 mg/mL bovine serum albumin (referred herein as DMEM/BSA). Subsequently, DMEM/BSA without or with different concentrations of unlabeled ligands and 80,000 cpm of [^{125}I]-NDP-MSH were added to each well, with the total volume of 1 ml, and then the cells were incubated at 37 °C for 1 h. The final concentration of various unlabeled ligands ranged from 10^{-11} to 10^{-6} M for NDP-MSH and THIQ, or from 10^{-10} to 10^{-5} M for α-MSH and ACTH (1-24). After incubation, the cells were washed twice with cold Hank's balanced salt solution containing 1 mg/mL BSA to terminate the reaction. Cells were then lysed by 0.5M NaOH and collected for radioactive assays by gamma counter (Cobra II Auto-Gamma, Packard Bioscience, Frankfurt, Germany).

(4) Ligand stimulated cAMP production

For intracellular cAMP evaluation, 48 h after transfection, HEK293T cells were washed twice with warm DMEM/BSA and then incubated with warm DMEM/BSA containing 0.5 mM isobutylmethylxanthine (Sigma-Aldrich) for 15 minutes. Subsequently, different concentrations of ligands were added to each well, with the total volume of 1 ml, to evaluate the ligand-stimulated intracellular cAMP levels. Final concentration of various unlabeled ligands ranged from 10^{-12} to 10^{-6} M. After 1 hour incubation, the reaction was terminated on the ice and intracellular cAMP was collected by adding 0.5 M percholoric acid containing 180 μg/ml theophylline (Sigma-Aldrich) and 0.72 M KOH/0.6 M $KHCO_3$ into each well. Intracellular cAMP levels were determined by radioimmunoassay as previously described [95] and ^{125}I-cAMP was iodinated via chloramine T method [95, 96].

3.2.6. Statistical analysis

SPSS19.0 software was used to calculate the mean and standard error of the mean (S.E.M.) of gene expression results and results are presented as mean ± S.E.M. Significant differences of gene expression were determined by one-way ANOVA followed by Duncan's multiple range test with the significance level set at $P < 0.05$. GraphPad Prism 4.0 software (San Diego, CA, USA) was used to calculate the ligand binding and cAMP signaling parameters such as maximal binding (B_{max}) and IC_{50} of ligand binding and maximal response (R_{max}) and EC_{50} of cAMP signaling. The significance of differences in B_{max}, IC_{50}, R_{max} and EC_{50} between *Lm*MC4R and hMC4R were determined by Student's *t*-test by GraphPad Prism 4.0 software.

3.3. Results

3.3.1. Nucleotide and deduced amino acid sequences of *Lm*MC4R

The bass *mc4r* gene sequence was identified from transcriptome databases (GenBank: SRR4409341/SRR4409397). The total cDNA sequence of bass *mc4r* was 1588 bp, containing an ORF of 981 bp that encoded a putative protein of 327 amino acids. We identified that the 5' and 3' untranslated region of bass *mc4r* was 493 bp and 114 bp, respectively. Like other GPCRs, *Lm*MC4R had seven putative hydrophobic transmembrane domains (TMDs) with three extracellular loops (ECLs) and three

intracellular loops (ICLs, Fig. 3.1). The deduced amino acid sequence of TMDs, ECLs and ICLs were significantly conserved to those of other species. The predicted amino acid sequence of *Lm*MC4R was 94, 88, 83, 82, 70, 70, and 70% identical to European sea bass (*Dicentrarchus labrax*), fugu (*Takifugu rubripes*), common carp (*Cyprinus carpio*), zebrafish (*Danio rerio*), human (*Homo sapiens*), chicken (*Gallus gallus*) and mouse (*Mus musculus*) MC4Rs, respectively (Fig. 3.2A). Phylogenetic tree analysis between *Lm*MC4R and MC4Rs in other vertebrates revealed that *Lm*MC4R was localized in a clade of teleost MC4Rs and was evolutionarily closer to European sea bass MC4R (Fig. 3.2B).

3.3.2. Bass *mc4r* mRNA tissue distribution and localization in brain

Bass *mc4r* mRNA expression in brain and peripheral tissues (pituitary, intestine, muscle, skin, spleen, liver, gill, kidney, stomach, heart and gonad) was analyzed by qRT-PCR (Fig. 3.3A). The expression of *18s* mRNA, a stable reference gene, was used as an internal control for normalization. Bass *mc4r* mRNA was highly expressed in the brain, followed by pituitary, liver and other peripheral tissues.

The relative mRNA expression of bass *mc4r* was evaluated in different brain regions (Fig. 3.3B). Higher *mc4r* mRNA expression was observed in telencephalon, diencephalon and pituitary gland (Fig. 3.3B). *In situ* hybridization showed that *mc4r* was localized in the ventral part of the ventral telencephalon (Vv) (Figs. 3.3D and 3.3E). The *mc4r*-expressing cells were observed in the brain regions of the central region of the olfactory bundle (Co)

(Figs. 3.3F and 3.3G), the lateral part of the dorsal telencephalon area (Dl) (Figs. 3.3H and 3.3I), and the medial part of the dorsal telencephalon part (Dm) (Figs. 3.3J and 3.3K). We also observed the localization of bass *mc4r* mRNA in cells of pituitary (Figs. 3.3L and 3.3M) and liver (Figs. 3.3N and 3.3O).

3.3.3. Change in bass *mc4r* mRNA expression in fasting challenge

To evaluate the potential physiological functions of bass *mc4r* in regulating energy homeostasis, we analyzed brain *mc4r* mRNA expressions in short-term and long-term fasting experiments. Short-term fasting did not change body weight (data not shown). Although there was no change at 1 h after fasting, there was significant decrease in *mc4r* expression at 6, 12 and 24 h (Fig. 3.4A). Expression of *agrp* was significantly decreased at 1, 12, and 24 h (Fig. 3.4B), and expression of *npy* was significantly decreased at 6 and 12h (Fig. 3.4C).

In long-term fasting experiment, when compared to the initial body weight (5.88 ± 0.26 g), bass in feeding group showed 10.44 g increase of body weight (16.32 ± 2.23 g), while bass of fasting group showed 0.15 g decrease of body weight (5.73 ± 0.07 g) (Fig. 3.4D). We observed that *mc4r* expression was significantly down-regulated (Fig. 3.4E), *agrp* mRNA expression was significantly up-regulated (Fig. 3.4F) while there was no significant change in *npy* expression (Fig. 3.4G).

3.3.4. Cell surface expression and ligand binding properties of *Lm*MC4R

The cell surface and total expressions of *Lm*MC4R were only ~2.1% to those of hMC4R, showing significant difference. Competitive ligand binding assays were performed to investigate the binding property of *Lm*MC4R. Different concentrations of unlabeled ligands including α-MSH, ACTH (1-24), NDP-MSH, THIQ and AgRP, were used to compete with a fixed amount of ^{125}I-NDP-MSH. Maximal binding value of the *Lm*MC4R was around 20% (22.58%) of that of the hMC4R (Fig. 3.5 and Table 3.2). Both hMC4R and *Lm*MC4R bound to NDP-MSH with the highest affinity. When unlabeled α-MSH, NDP-MSH ACTH (1-24) or AgRP was used as the ligand, *Lm*MC4R showed significantly lower IC_{50} values compared to those of hMC4R (Table 3.2). When THIQ, Ipsen 5i and ML00253764 were used as the unlabeled competitors, *Lm*MC4R was not able to displace ^{125}I-NDP-MSH, whereas dose-dependent displacement of ^{125}I-NDP-MSH binding to the hMC4R was observed (Figs. 3.5D, 3.8A and 3.8B).

3.3.5. Signaling properties of *Lm*MC4R

Dose-dependent increase of intracellular cAMP was observed when *Lm*MC4R was stimulated by NDP-MSH, α-MSH, ACTH (1-24) and THIQ (Fig. 3.6). AgRP served as the inverse agonist (Fig. 3.7B). However, the Ispen 5i and ML00253764 significantly decreased *Lm*MC4R basal cAMP levels (Fig. 3.8C). The maximal responses of *Lm*MC4R in response to NDP-MSH, α-MSH, and ACTH were 144.57 ± 8.65%, 216.86 ± 16.88% and 125.56 ± 5.45%, respectively, of those of hMC4R, whereas the maximal response of

*Lm*MC4R in response to THIQ was 57.78 ± 5.32% of that of hMC4R (Fig. 3.6 and Table 3.3). EC_{50}s of NDP-MSH and THIQ for *Lm*MC4R were significantly higher than those for hMC4R, and EC_{50}s of α-MSH and ACTH (1-24) for *Lm*MC4R and hMC4R were not significantly different (Fig. 3.6 and Table 3.3).

3.4. Discussion

In this study, we demonstrated that spotted sea bass *mc4r* encoded a protein of 327 amino acids with seven transmembrane domains and conversed motifs such as PMY, DRY, and DPIIY (DPxxY) (Fig. 3.1). Compared to transmembrane domains, extracellular N-terminal domain and ECLs were less conservative (Fig. 3.2). Similar results have also been reported in other teleosts [128-130, 146, 147]. Cys residues have been shown to be critical for MC4R integrity possibly by forming disulfide bonds [148]. We identified 15 Cys residues in *Lm*MC4R, as in other teleost MC4Rs [127, 147], suggesting that the number of Cys residues was highly conserved in MC4Rs during teleost evolution. Amino acid sequence of *Lm*MC4R was 94% identical to European sea bass MC4R, 80% identical to several other teleost MC4Rs including zebrafish, fugu and carp, and was approximately 70% identical to mammalian MC4Rs (Fig. 3.2).

Wo observed the highest *mc4r* expression in brain (Fig. 3.3). This is consistent with previous studies that nonmammalian *MC4Rs* are also abundantly expressed in brain [6]. Expression patterns of the teleost *mc4r* are much wider when compared to those in mammals. In addition to brain, teleost *mc4r* are also expressed in pituitary and certain

peripheral tissues including eyes, liver, gonads, spleen and gastrointestinal tract [6]. The spotted sea bass *mc4r* was also highly expressed in pituitary, similar to findings in barfin flounder, goldfish, zebrafish and European sea bass [6]. Recent studies showed teleost MC4Rs might play important role in regulating gonadal development [129, 130]. In this study, we observed that *mc4r* expression in spotted sea bass gonad was low (Fig. 3.3). Taken together, these results suggested that wider expression of teleost *mc4r* might be associated with roles in regulating multiple physiological functions.

In mice, changes in food intake represent 60% of the total effect of the MC4R in regulating energy homeostasis [6]. In Mexican cavefish (*Astyanax mexicanus*), *mc4r* mutations associated with signaling efficiency contribute to physiological adaptations to nutrient-poor conditions by increasing appetite, growth, and starvation resistance [132]. We observed short-term fasting led to down-regulation of *mc4r* with fluctuating changes in *agrp* and *npy* expression while long-term fasting resulted in down regulated *mc4r* with up-regulated *agrp* (Fig. 3.4). All these results showed the conserved function of MC4R in regulating food intake [6]. Further studies need to investigate the distinct functions of AGRP or NPY neurons in regulating food intake with MC4R due to the fact they showed different transcriptional patterns during fasting (Fig. 3.4).

Detailed pharmacological studies were further performed on *Lm*MC4R. We observed that the cell surface expression of *Lm*MC4R was significantly lower than that of hMC4R, which might explain the differences of total binding between *Lm*MC4R and hMC4R. Ligand binding experiments also showed that *Lm*MC4R bound to α-MSH and ACTH (1-

24) with similar affinities (Fig. 3.5). Compared with hMC4R, *Lm*MC4R showed significantly higher binding affinity to NDP-MSH (~60-fold higher), α-MSH (~20-fold higher), and ACTH analogue (1-24) (~20-fold higher) (Fig. 3.5), consistent with previous studies of swamp eel, spotted scat, orange-spotted grouper, fugu and rainbow trout MC4Rs [129-131, 151, 152].

In cAMP signaling assays, α-MSH and ACTH (1-24) stimulated *Lm*MC4R and hMC4R with similar potencies (Fig. 3.6). THIQ could bind to hMC4R and displace the ^{125}I-NDP-MSH in a dose-dependent manner, suggesting that binding sites of THIQ and NDP-MSH were overlapping. THIQ could not displace^{125}I-NDP-MSH binding at *Lm*MC4R; however, THIQ stimulated intracellular cAMP accumulation at *Lm*MC4R with an EC_{50} of 63.88 nM, which was significantly higher than that of hMC4R. We propose that THIQ might act as an allosteric agonist at *Lm*MC4R, similar to our previous studies in grass carp and swamp eel [129, 130].

In agreement with previous studies that teleost MC4Rs showed high constitutive activity in cAMP pathway [128-131], this study observed that *Lm*MC4R had approximately 8-fold higher constitutive activity than that of hMC4R (Fig. 3.6, Table 3.3). N-termini act as an important modulator in regulating constitutive activities in GPCRs [153-155]. Although amino acid sequences of MC4Rs are conserved from mammals to teleosts, N-termini of *Lm*MC4R and other teleost MC4Rs were less conserved to those of hMC4R, raising the possibility that variations of residues in N-termini might lead to high constitutive activities in teleost. Indeed, hMC4R has also been shown to have constitutive activity [156]

and mutations leading to decreased constitutive activity or other loss-of-functions are believed to be associated with obesity pathogenesis [124, 157, 158]. However, in agriculture (aquaculture), the farmed animals with lower MC4R constitutive activity may show a higher food efficiency, lower basal metabolism and faster weight gain, increasing the economic benefits of agriculture (aquaculture). Inverse agonists that decrease fish MC4R constitutive activity might be used in aquaculture.

Table 3.1 The primers of *mc4r*, *agrp*, *npy* and *18s* in spotted sea bass

Primer name	Primer sequence (5'-3')	Application
mc4r-f	CGGTGCTCATCTGCCTCATC	qRT-PCR
mc4r-r	CTTCATGTTGGCTCGCTGGT	qRT-PCR
mc4r-f	CGCATTTAGGTGACACTATAGAAGCGAAGACTTATCAGGCGAGGAC	ISH
mc4r-r	CCGTAATACGACTCACTATAGGGAGACAAGGAGGATGGTGAGGGTG	ISH
agrp-f	GATGGACACAGGCTCCTACGAC	qRT-PCR
agrp-r	GGCATTGAAGAAGCGGCA	qRT-PCR
npy-f	GAGGGATACCCGATGAAACCG	qRT-PCR
npy-r	CCTCTTTCCATACCTCTGTCTCG	qRT-PCR
18s-f	GGGTCCGAAGCGTTTACT	qRT-PCR
18s-r	TCACCTCTAGCGGCACAA	qRT-PCR

Table 3.2 The ligand binding properties of *Lm*MC4R

	B_{max} (%)	NDP-MSH	α-MSH	ACTH	THIQ	AgRP
		IC_{50} (nM)	IC_{50} (nM)	IC_{50} (nM)	IC_{50} (nM)	IC_{50} (nM)
hMC4R	100	18.467 ± 0.853	576.700 ± 0.374	457.833 ± 116.817	156.667 ± 16.040	417.167 ± 116.045
*Lm*MC4R	22.657	0.305 ± 0.032[b]	31.947 ± 4.859[b]	24.660 ± 5.545[a]	N/A[c]	4.768 ±0.391

[a] Significantly different from the parameter of hMC4R, $P<0.05$;

[b] Significantly different from the parameter of hMC4R, $P<0.001$;

[c] Could not be determined.

Table 3.3 The cAMP signaling properties of *Lm*MC4R

	Basal (%)	NDP-MSH		α-MSH		ACTH		THIQ	
		EC_{50} (nM)	R_{max} (%)	EC_{50} (nM)	R_{max} (%)	EC_{50} (nM)	R_{max} (%)	EC_{50} (nM)	R_{max} (%)
hMC4R	100	1.216 ± 0.077	100	2.690 ± 0.374	100	2.132 ± 0.486	100	2.308 ± 0.240	100
*Lm*MC4R	891 ± 251	5.094 ± 1.058[a]	144.568 ± 8.653	5.200 ± 0.796	216.856 ± 16.877	2.717 ± 0.507	125.559 ± 5.454	63.883 ± 11.236[b]	57.782 ± 5.323

[a] Significantly different from the parameter of hMC4R, $P<0.05$;

[b] Significantly different from the parameter of hMC4R, $P<0.01$.

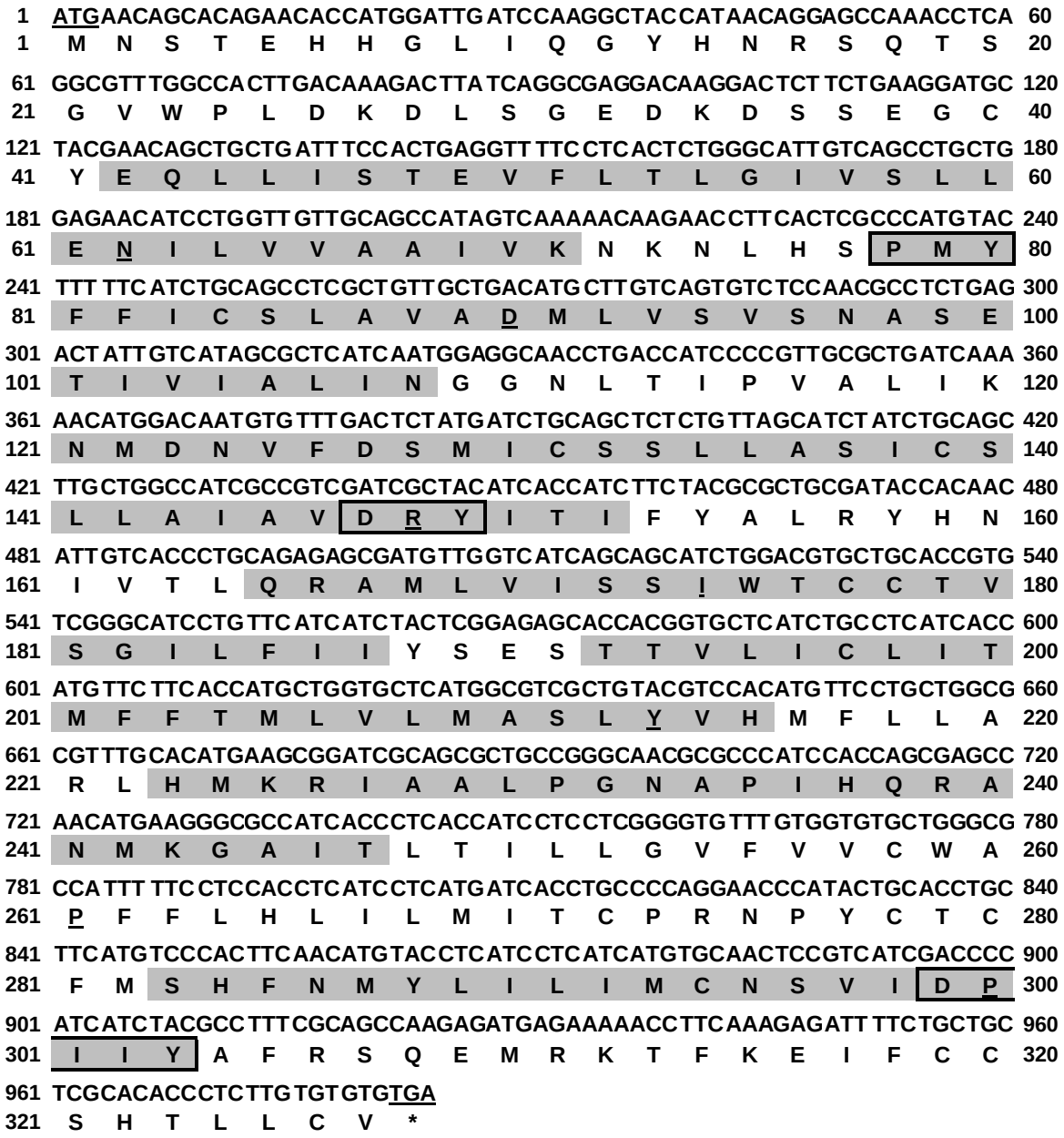

Fig. 3.1. Nucleotide and deduced amino acid sequence of *Lm*MC4R.

Positions of nucleotide and amino acid sequences are indicated on both sides. The seven TMDs are shaded in grey. The conserved motifs (PMY, DRY, and DPIIY) are highlighted in boxes. Underlines show initiation codon and most conserved residues in each TMD. Asterisk (*) denotes stop codon.

A

```
Lateolabrax maculatus (spotted sea bass)  M-NSTEHHGL IQGYHNRSQT SGVWPLDKDL SGEDKDSSEG CYEQLLISTE VFLTLGIVSL LENILVVAAI VKNKNLHSPM  79
Homo sapiens (human)                      MVNSTHR-GM HTSLHLWNRS SYRLHSNASE SLGKGYSDGG CYEQLFVSPE VFVTLGVISL LENILVIVAI AKNKNLHSPM  79
Mus musculus (mouse)                      M-NSTHHHGM YTSLHLWNRS SYGLHSNASE SLGKGHPDGG CYEQLFVSPE VFVTLGVISL LENILVIVAI AKNKNLHSPM  79
Gallus gallus (chicken)                   M-NFTQHRGT LQPLHFWNQS N-GLHRGASE PSAKGHSSGG CYEQLFVSPE VFVTLGIISL LENVLVIVAI AKNKNLHSPM  78
Takifugu rubripes (fugu)                  M-NATDPPGR VQDFSNGSQT P-----ETDF PNEEKESSTG CYEQMLISTE VFLTLGIISL LENILVVAAI VKNKNLHSPM  74
Dicentrarchus labrax (European seabass )  M-NTTEAHGL IHGYHNRSQT SGILPLNKDL SAEEKDSSTG CYEQLLISPE VFLTLGIVSL LENILVVAAI IKNKNLHSPM  79
Cyprinus carpio (carp)                    M-NTSHHHGL HHSYRNHSQ- -GALPVGKP- DQGERGSASG CYEQLLISTE VFLTLGLVSL LENILVIAAI IKNKNLHSPM  76
Danio rerio (zebrafish)                   M-NTSHHHGL HHSFRNHSQ- -GALPVGKP- SHGDRGSASG CYEQLLISTE VFLTLGLVSL LENILVIAAI VKNKNLHSPM  76

                                                  TM2                                                 TM3
Lateolabrax maculatus (spotted sea bass)  YFFICSLAVA DMLVSVSNAS ETIVIALING GNLTIPVALI KNMDNVFDSM ICSSLLASIC SLLAIAVDRY ITIFYALRYH  159
Homo sapiens (human)                      YFFICSLAVA DMLVSVSNGS ETIVITLLNS TD-TDAQSFT VNIDNVIDSV ICSSLLASIC SLLSIAVDRY FTIFYALQYH  158
Mus musculus (mouse)                      YFFICSLAVA DMLVSVSNGS ETIVITLLNS TD-TDAQSFT VNIDNVIDSV ICSSLLASIC SLLSIAVDRY FTIFYALQYH  158
Gallus gallus (chicken)                   YFFICSLAVA DMLVSVSNGS ETIVITLLNN ID-TDAQSFT INIDNVIDSV ICSSLLASIC SLLSIAVDRY FTIFYALQYH  157
Takifugu rubripes (fugu)                  YFFICSLAVA DMLVSVSNAS ETIVIALINS GTLTIPATLI KSMDNVFDSM ICSSLLASIC SLLAIAVDRY ITIFYALRYH  154
Dicentrarchus labrax (European seabass )  YFFICSLAVA DMLVSVSNAS ETIVIALING GKLTIPVQLI KSMDNVFDSM ICSSLLASIC SLLAIAVDRY ITIFYALRYH  159
Cyprinus carpio (carp)                    YFFICSLAVA DLLVSVSNAS ETVVMALITG GNLTNRESII KNMDNIFDSM ICSSLLASIW SLLAIAVDRY ITIFYALRYH  159
Danio rerio (zebrafish)                   YFFICSLAVA DLLVSVSNAS ETVVMALITG GNLTNRESII KNMDNVFDSM ICSSLLASIW SLLAIAVDRY ITIFYALRYH  159

                                                  TM4                                                 TM5
Lateolabrax maculatus (spotted sea bass)  NIVTLQRAML VISSIWTCCT VSGILFIIYS ESTTVLICLI TMFFTMLVLM ASLYVHMFLL ARLHMKRIAA LPGNAPIHQR  239
Homo sapiens (human)                      NIMTVKRVGI IISCIWAACT VSGILFIIYS DSSAVIICLI TMFFTMLALM ASLYVHMFLM ARLHIKRIAV LPGTGAIRQG  238
Mus musculus (mouse)                      NIMTVRRVGI IISCIWAACT VSGVLFIIYS DSSAVIICLI SMFFTMLVLM ASLYVHMFLM ARLHIKRIAV LPGTGTIRQG  238
Gallus gallus (chicken)                   NIMTVKRVGV IITCIWAACT VSGILFIIYS DSSVVIICLI SMFFTMLILM ASLYVHMFMM ARMHIKKIAV LPGTGPIRQG  237
Takifugu rubripes (fugu)                  NIVTLRRASL VISSIWTCCT VSGVLFIVYS ESTTVLICLI TMFFTMLVLM ASLYVHMFLL ARLHMKRIAA MPGNAPIHQR  235
Dicentrarchus labrax (European seabass )  NIVTLRRAML VISSIWTCCI VSGILFIIYS ESTTVLICLI TMFFTMLVLM ASLYVHMFLL ARLHMKRIAA LPGNAPIHQR  239
Cyprinus carpio (carp)                    NIMTQRRAGT IITCIWTFCT VSGVLFIVYS ESTTVLICLI SMFFTMLALM ASLYVHMFLL ARLHMKRIAA LPGNAPIWQA  236
Danio rerio (zebrafish)                   NIMTQRRAGT IITCIWTFCT VSGVLFIVYS ESTTVLICLI SMFFTMLALM ASLYVHMFLL ARLHMKRIAA LPGNGPIWQA  236

                                                  TM6                                                 TM7
Lateolabrax maculatus (spotted sea bass)  ANMKGAITLT ILLGVFVVCW APFFLHLILM ITCPRNPYCT CFMSHFNMYL ILIMCNSVID PIIYAFRSQE MRKTFKEIFC  319
Homo sapiens (human)                      ANMKGAITLT ILIGVFVVCW APFFLHLIFY ISCPQNPYCV CFMSHFNLYL ILIMCNSIID PLIYALRSQE LRKTFKEIIC  318
Mus musculus (mouse)                      TNMKGAITLT ILIGVFVVCW APFFLHLLFY ISCPQNPYCV CFMSHFNLYL ILIMCNAVID PLIYALRSQE LRKTFKEIIC  318
Gallus gallus (chicken)                   ANMKGAITLT ILIGVFVVCW APFFLHLIFY ISCPYNPYCV CFMSHFNFYL ILIMCNSIID PLIYAFRSQE LRKTFKEIIC  317
Takifugu rubripes (fugu)                  ANLKGAITLT ILLGVFVVCW APFFLHLILM ITCPKNPYCT CFMSHFNMYL ILIMCNSVID PIIYAFRSQE MRKTFKEIFC  315
Dicentrarchus labrax (European seabass )  ANMKGAITLT ILIGVFVVCW APFFLHLILM ITCPRNPYCT CFMSQFNMYL ILIMCNSVID PIIYAFRSQE MRKTFKEIFC  319
Cyprinus carpio (carp)                    ANMKGAITIT ILLGVFVVCW APFFLHLILM ISCPRNPYCI CFMSHFNMYL ILIMCNSVID PLIYAFRSQE MRKTFKEICC  316
Danio rerio (zebrafish)                   ANMKGAITIT ILLGVFVVCW APFFLHLILM ISCPRNPYCV CFMSHFNMYL ILIMCNSVID PLIYAFRSQE MRKTFKEICC  316

Lateolabrax maculatus (spotted sea bass)  CSHTL--LCV -----  327
Homo sapiens (human)                      C-YPLGGLCD LSSRY  332
Mus musculus (mouse)                      F-YPLGGICE LSSRY  332
Gallus gallus (chicken)                   -CCNLRGLCD LPGKY  331
Takifugu rubripes (fugu)                  CSQML--VCM -----  323
Dicentrarchus labrax (European seabass )  CSHAL--LCV -----  327
Cyprinus carpio (carp)                    CWYGLTSLCV -----  326
Danio rerio (zebrafish)                   CWYGLASLCV -----  326
```

B

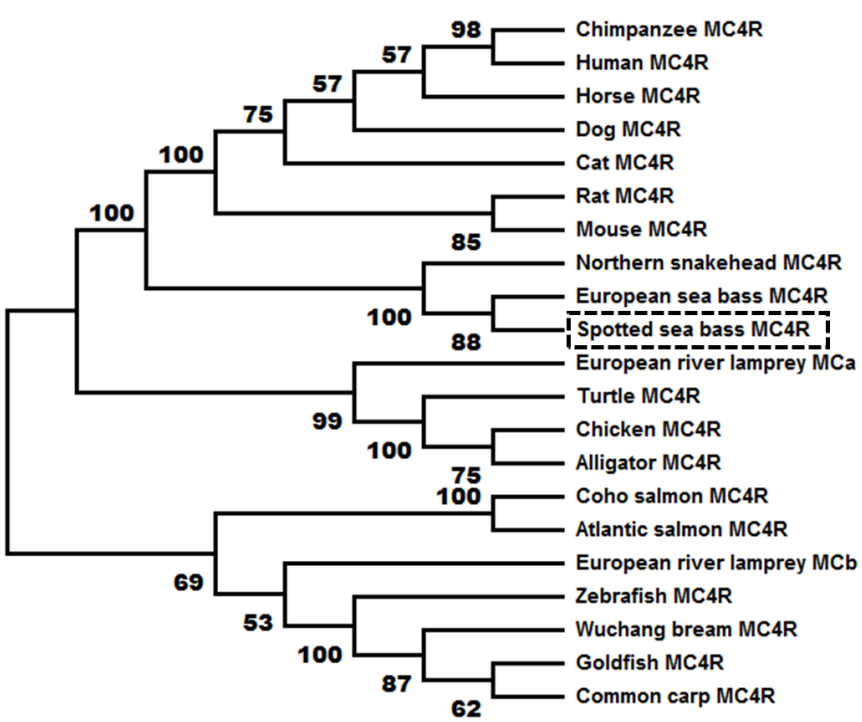

Fig. 3.2. Comparison of amino acid sequences between *Lm*MC4R and MC4Rs from other species (A) and phylogenetic tree of MC4R proteins (B).

In Fig. 2A, amino acids in shaded boxes indicate putative TMD 1-7, the most conserved residues in each TMD are underlined. In Fig. 2B, trees were constructed using the neighbor-joining (NJ) method. Box shows *Lm*MC4R. GenBank accession numbers: alligator (XP_006025279.1); Atlantic salmon (XP_014036044.1); cat (BBD19891.1); chicken (NP_001026685.1); chimpanzee (PNI69802.1); coho salmon (XP_020349696.1); common carp (CBX89936.1); dog (NP_001074193.1); European river lamprey MCRa (ABB36647.1); European river lamprey MCRb (ABB36648.1); European seabass (CBN82190.1); goldfish (CAD58853.1); horse (XP_001489706.1); human (NP_005903.2); mouse (NP_058673.2); Northern snakehead (AMM02541.1); rat (NP_037231.1); turtle (XP_024059247.1); Wuchang bream (AWA81516.1); zebrafish (NP_775385.1).

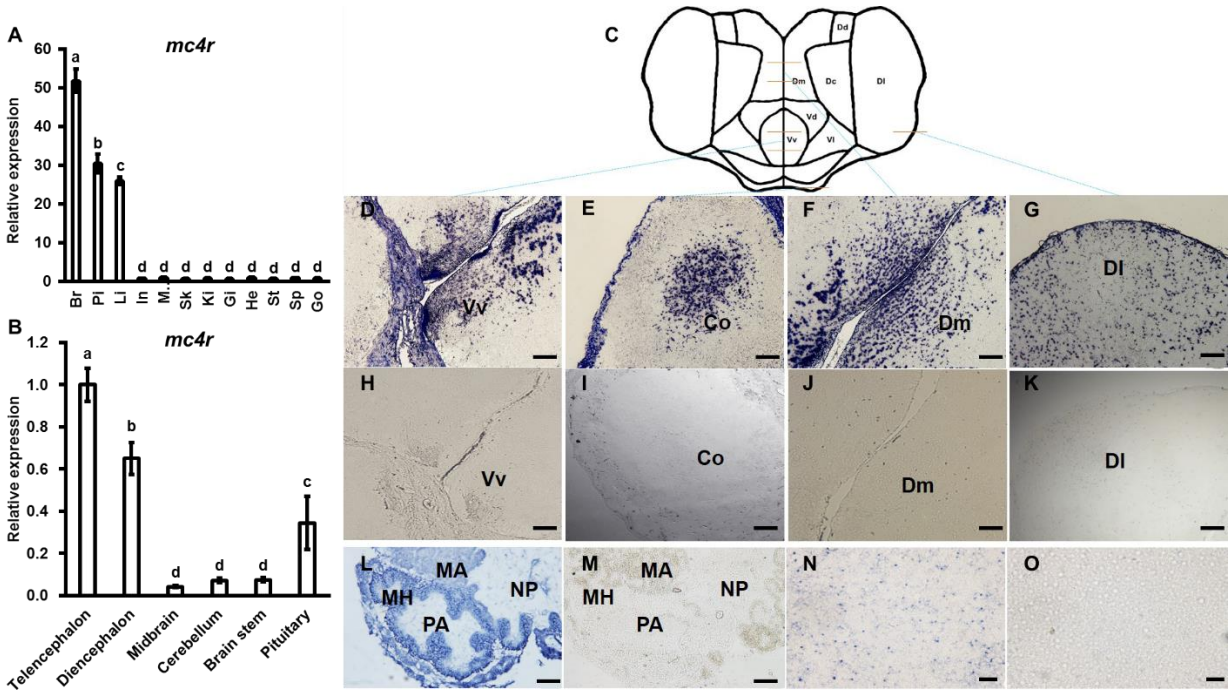

Fig. 3.3. Expression of bass *mc4r* mRNA in various tissues (A) and brain regions (B) and localization in brain (D - K), pituitary (L and M) and liver (N and O).

Data are presented as means ± S.E., n = 6. Different letters indicate significant difference ($P < 0.05$, one-way ANOVA followed by Duncan's multiple range test). In, intestines; Pi, pituitary; Mu, muscle; Br, brain; Sk, skin; Sp, spleen; Li, liver; Gi, gill; Ki, kidney; St, stomach; He, heart; Go, gonad. The structure and cut regions of telencephalon is shown in Fig. 3C. Fig. 3D - 3K, 3L - 3M and 3N - 3O show the bass *mc4r* mRNA localization in brain, pituitary and liver, respectively. Hybridization of sense bass *mc4r*-cRNA probe did not display specific signals in the brain samples (H-K, M and O), showing specificity of the signal. Vv, ventral telencephalon; Co, central region of the olfactory bundle; Dl, lateral part of the dorsal telencephalon area; Dm, medial part of the dorsal telencephalon part. PA, pro-adenohypophysis; MH, meso-adeno hypophysis; MA, meta adenohypophysis;

NP, neurohypophysis. Scale bars of figs. D - K indicate 50 μm and figs. L - O indicate 20 μm.

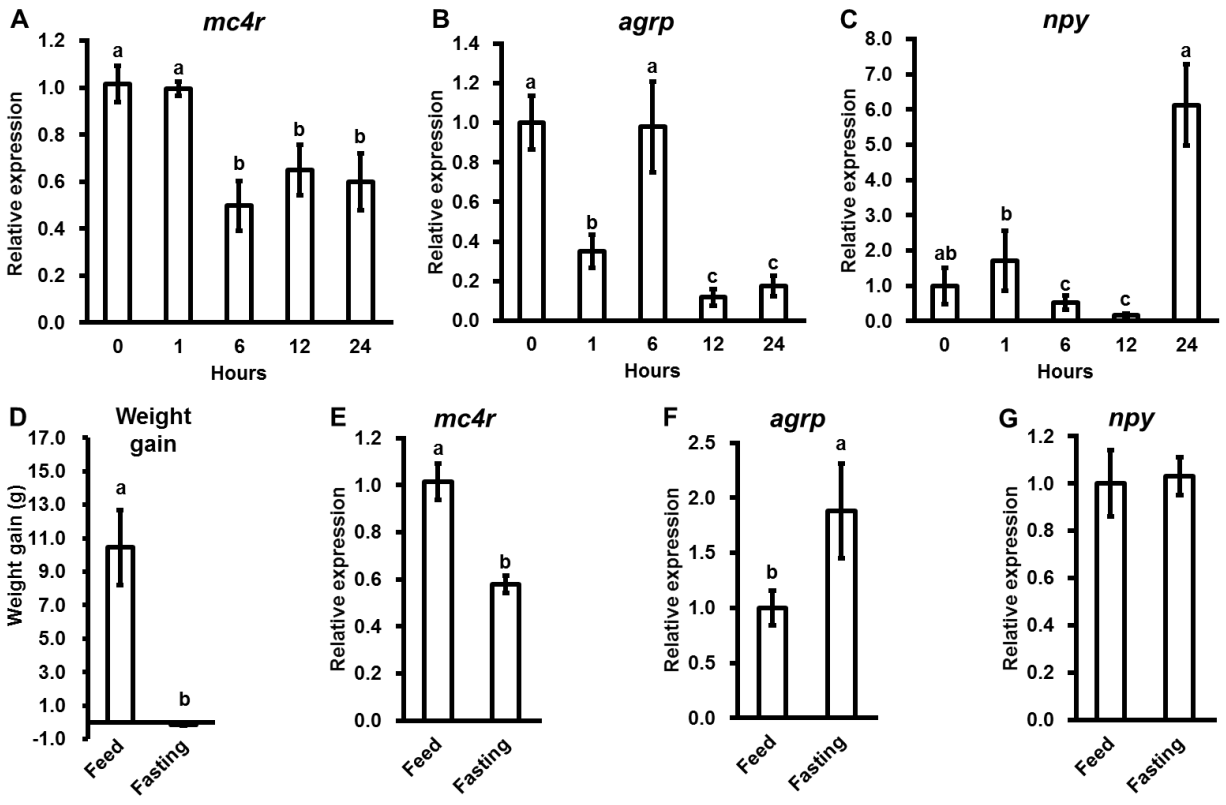

Fig. 3.4. Body weight of spotted sea bass in long-term fasting challenge (A). The relative mRNA expression of brain *mc4r, agrp* and *npy* during long-term (B, C, D) and short-term (E, F, G) fasting challenge.

Data are presented as means ± S.E., n = 6. Different letters indicate significant difference ($P < 0.05$, one-way ANOVA followed by Duncan's multiple range test).

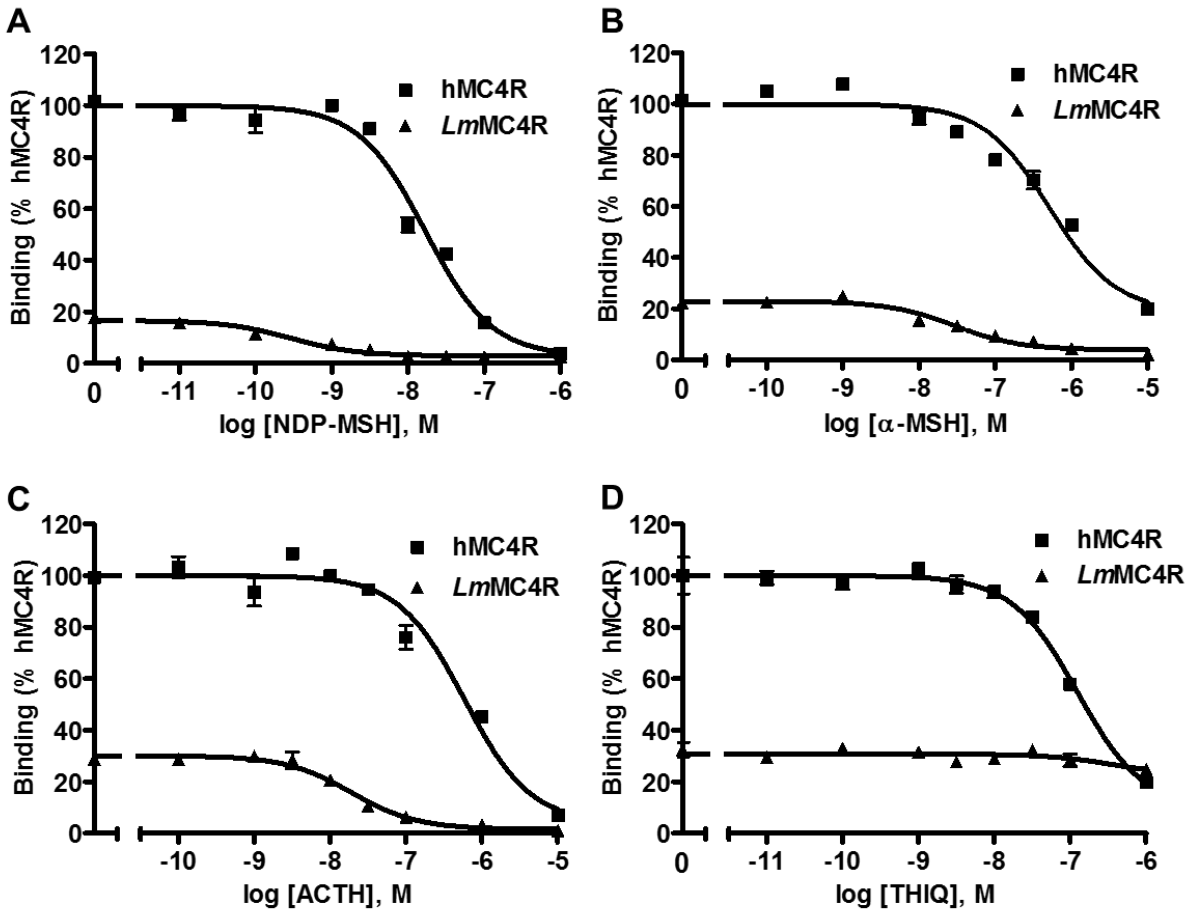

Fig. 3.5. Ligand binding properties of *Lm*MC4R.

HEK293T cells were transiently transfected with hMC4R or *Lm*MC4R plasmids. Forty-eight hours after transfection, different concentrations of unlabeled NDP-MSH (A), α-MSH (B), ACTH (1-24) (C) and THIQ (D) were used to displace the binding of ^{125}I-NDP-MSH, rescpectively. Data are expressed as % of hMC4R binding ± range from duplicate measurements within one experiment. The "error bar" on each dot represents the "distribution" of duplicate measurements within one experiment. The curves are representative of 3 independent experiments. All experiments were performed at least three times with similar results.

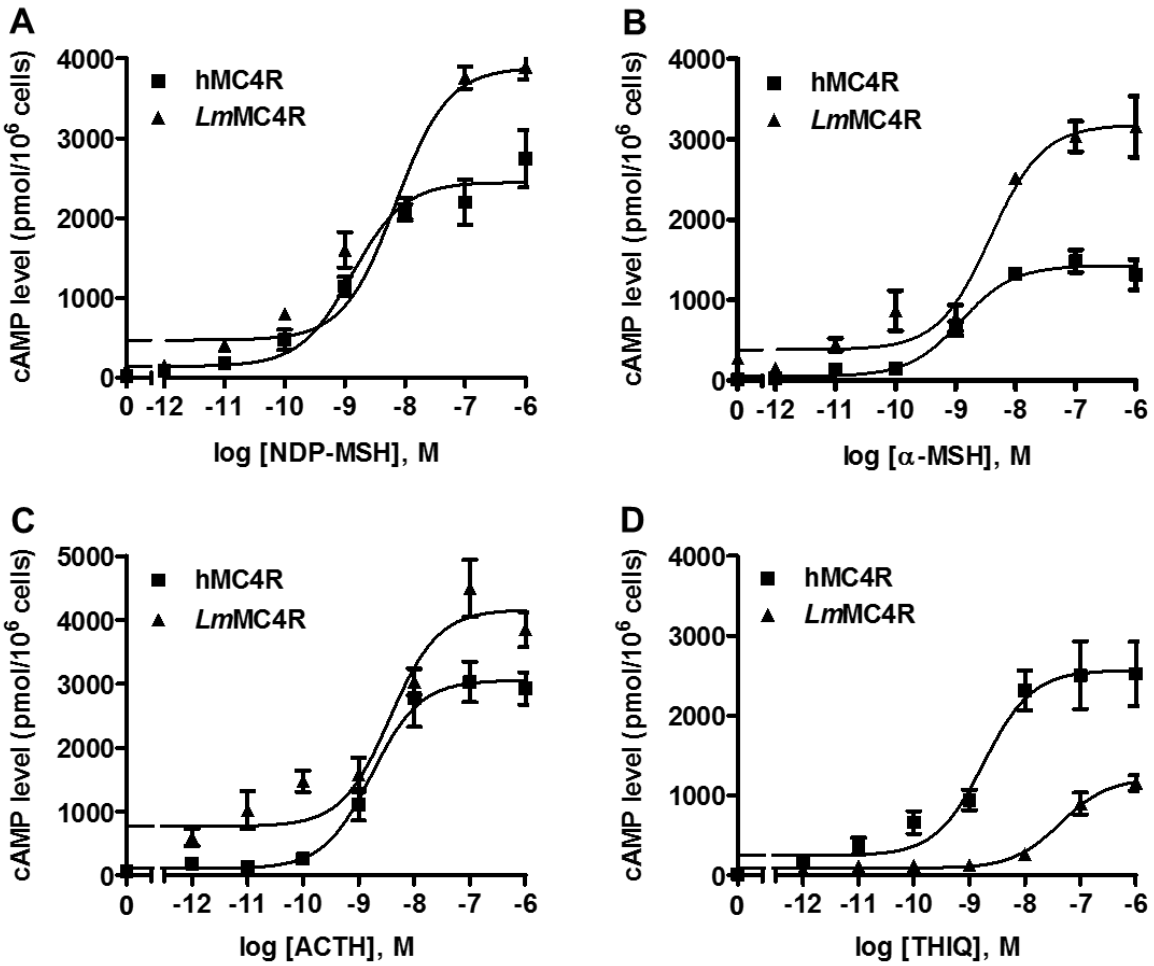

Fig. 3.6. Signaling properties of *Lm*MC4R.

HEK293T cells were transiently transfected with hMC4R or *Lm*MC4R plasmids. Forty-eight hours after transfection, different concentrations of NDP-MSH, α-MSH, ACTH (1–24) or THIQ was used to stimulate the cells transfected with hMC4R or *Lm*MC4R. Data are expressed as mean ± SEM from triplicate measurements within one experiment. The "error bar" on each dot represents the "distribution" of triplicate measurements within one experiment. The curves are representative of 3 independent experiments. All experiments were performed at least three times with similar results.

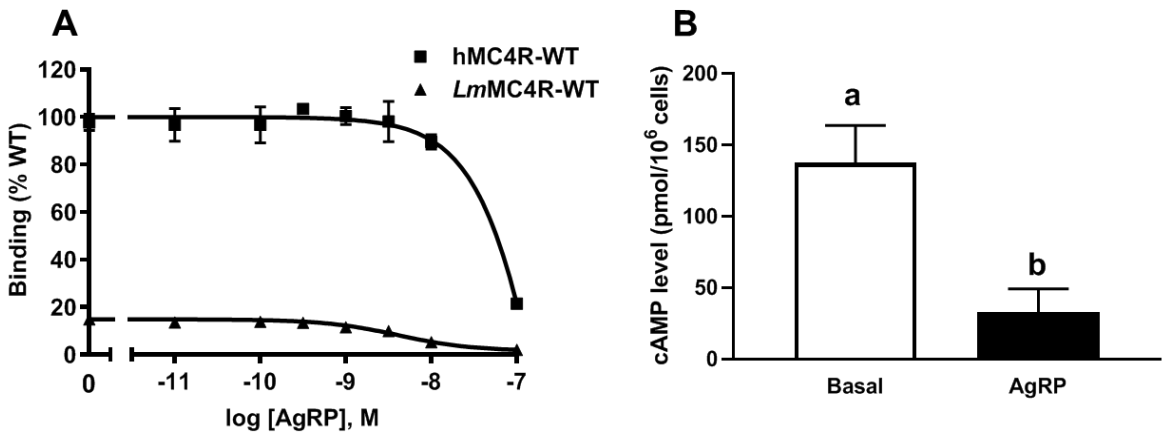

Fig. 3.7. Ligand binding (A) and siganling properties (B) of AgRP at *Lm*MC4R.

HEK293T cells were transiently transfected with hMC4R or *Lm*MC4R plasmids. Forty-eight hours after transfection, different concentrations of AgRP were used to (A) displace the binding of ^{125}I-NDP-MSH or (B) stimulate (10^{-8} M) the cells transfected with *Lm*MC4R. Data are from triplicate measurements within one experiment. The curves are representative of 3 independent experiments. Different letters indicate significant difference ($P < 0.05$, one-way ANOVA followed by Duncan's multiple range test).

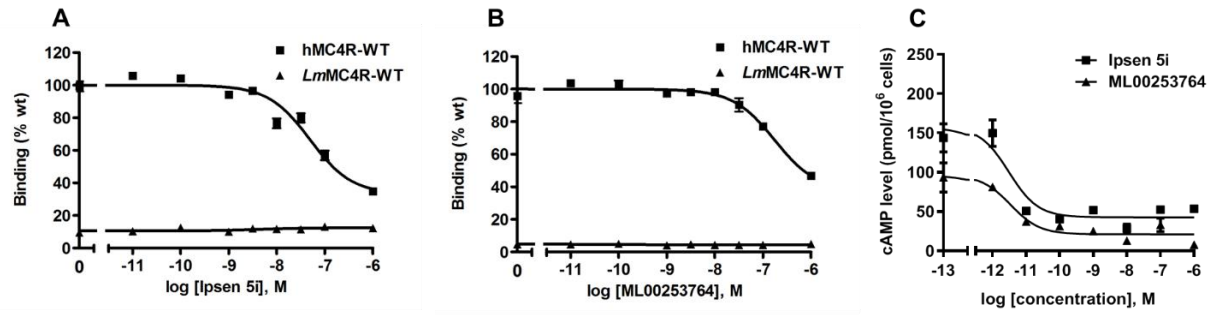

Fig. 3.8. Allosteric modulatory activity of Ipsen 5i or ML00253764 at LmMC4R. HEK293T cells were transiently transfected with hMC4R or *Lm*MC4R plasmids. Forty-eight hours after transfection, different concentrations of Ipsen 5i or ML00253764 were used to displace the binding of 125I-NDP-MSH or stimulate the cells transfected with *Lm*MC4R. The curves are representative of 3 independent experiments.

Conclusions

Firstly, we showed Zn^{2+} and Cu^{2+} acted as biased allosteric modulators at hMC4R. The Zn^{2+} and Cu^{2+} selectively modulated cAMP signaling but not the ERK1/2 signaling. The Zn^{2+} acted as an allosteric modulator at WT hMC4R, enhancing the binding affinity but decreasing the potency of α-MSH. Cu^{2+} acted as an allosteric enhancer in a lower concentration, but an allosteric inhibitor in a high concentration. The Zn^{2+} and Cu^{2+} failed to impact the RM493-induced cAMP accumulation probably because RM493 exerts distinct binding site with α-MSH at hMC4R. The D122, one of the three binding sites of calcium, also acted as a potential binding site of Zn^{2+}. Our study might provide new opportunities for the development of the drugs with improved profile by coordinating with metal ions.

Secondly, we investigated the cloning, tissue distribution, physiology, and pharmacology of spotted sea bass MC4R (*Lm*MC4R). We showed the spotted sea bass *mc4r* consisted of a 984 bp open reading frame encoding a protein of 327 amino acids. The spotted sea bass *mc4r* transcripts were highly expressed in the brain, followed by pituitary and liver. Brain *mc4r* transcripts were down-regulated in long-term and short-term fasting challenges. The *Lm*MC4R was a functional receptor with lower maximal binding and higher basal activity than hMC4R. THIQ, Ipsen 5i and ML00253764 were not able to displace ^{125}I-NDP-MSH but could affect intracellular cAMP accumulation, suggesting that they were allosteric ligands for *Lm*MC4R. In summary, we cloned spotted sea bass MC4R, and showed that it had different pharmacological properties compared

to hMC4R, and potentially different functions.

References

[1] B. Zarzycka, S.A. Zaidi, B.L. Roth, V. Katritch, Harnessing ion-binding sites for GPCR pharmacology, Pharmacol Rev, 71 (2019) 571-595.

[2] Y.X. Tao, Inactivating mutations of G protein-coupled receptors and diseases: Structure-function insights and therapeutic implications, Pharmacol Ther, 111 (2006) 949-973.

[3] A.D. Howard, G. McAllister, S.D. Feighner, Q. Liu, R.P. Nargund, L.H.T. Van der Ploeg, A.A. Patchett, Orphan G-protein-coupled receptors and natural ligand discovery, Trends Pharmacol Sci, 22 (2001) 132-140.

[4] J. Bockaert, J.P. Pin, Molecular tinkering of G protein-coupled receptors: an evolutionary success, EMBO J, 18 (1999) 1723-1729.

[5] S. Takeda, S. Kadowaki, T. Haga, H. Takaesu, S. Mitaku, Identification of G protein-coupled receptor genes from the human genome sequence, FEBS Lett, 520 (2002) 97-101.

[6] Y.X. Tao, The melanocortin-4 receptor: Physiology, pharmacology, and pathophysiology, Endocr Rev, 31 (2010) 506-543.

[7] R.D. Cone, Studies on the physiological functions of the melanocortin system, Endocr Rev, 27 (2006) 736-749.

[8] P. Valverde, E. Healy, I. Jackson, J.L. Rees, A.J. Thody, Variants of the melanocyte-stimulating hormone receptor gene are associated with red hair and fair skin in humans,

Nat Genet, 11 (1995) 328-330.

[9] K.G. Mountjoy, L.S. Robbins, M.T. Mortrud, R.D. Cone, The cloning of a family of genes that encode the melanocortin receptors, Science, 257 (1992) 1248-1251.

[10] A.S. Chen, D.J. Marsh, M.E. Trumbauer, E.G. Frazier, X.M. Guan, H. Yu, C.I. Rosenblum, A. Vongs, Y. Feng, L. Cao, J.M. Metzger, A.M. Strack, R.E. Camacho, T.N. Mellin, C.N. Nunes, W. Min, J. Fisher, S. Gopal-Truter, D.E. MacIntyre, H.Y. Chen, L.H. Van der Ploeg, Inactivation of the mouse melanocortin-3 receptor results in increased fat mass and reduced lean body mass, Nat Genet, 26 (2000) 97-102.

[11] S.J. Getting, Y. Riffo-Vasquez, S. Pitchford, M. Kaneva, P. Grieco, C.P. Page, M. Perretti, D. Spina, A role for MC3R in modulating lung inflammation, Pulm Pharmacol Ther, 21 (2008) 866-873.

[12] K. Begriche, C. Girardet, P. McDonald, A.A. Butler, Melanocortin-3 receptors and metabolic homeostasis, Prog Mol Biol Transl Sci, 114 (2013) 109-146.

[13] W. Chen, M.A. Kelly, X. Opitz-Araya, R.E. Thomas, M.J. Low, R.D. Cone, Exocrine gland dysfunction in MC5-R-deficient mice: evidence for coordinated regulation of exocrine gland function by melanocortin peptides, Cell, 91 (1997) 789-798.

[14] A.I. Smith, J.W. Funder, Proopiomelanocortin processing in the pituitary, central nervous system, and peripheral tissues, Endocr Rev, 9 (1988) 159-179.

[15] R.M. Dores, S. Lecaude, Trends in the evolution of the proopiomelanocortin gene, Gen Comp Endocrinol, 142 (2005) 81-93.

[16] A.A. Butler, C. Girardet, M. Mavrikaki, J.L. Trevaskis, H. Macarthur, D.L. Marks, S.A. Farr, A life without hunger: the ups (and downs) to modulating melanocortin-3 receptor

signaling, Front Neurosci, 11 (2017) 128.

[17] W. Fan, B.A. Boston, R.A. Kesterson, V.J. Hruby, R.D. Cone, Role of melanocortinergic neurons in feeding and the agouti obesity syndrome, Nature, 385 (1997) 165-168.

[18] D. Lu, D. Willard, I.R. Patel, S. Kadwell, L. Overton, T. Kost, M. Luther, W. Chen, R.P. Woychik, W.O. Wilkison, R.D. Cone, Agouti protein is an antagonist of the melanocyte-stimulating-hormone receptor, Nature, 371 (1994) 799-802.

[19] T.M. Fong, C. Mao, T. MacNeil, R. Kalyani, T. Smith, D. Weinberg, M.R. Tota, L.H. Van der Ploeg, ART (protein product of agouti-related transcript) as an antagonist of MC-3 and MC-4 receptors, Biochem Biophys Res Commun, 237 (1997) 629-631.

[20] M.M. Ollmann, B.D. Wilson, Y.K. Yang, J.A. Kerns, Y. Chen, I. Gantz, G.S. Barsh, Antagonism of central melanocortin receptors in vitro and in vivo by agouti-related protein, Science, 278 (1997) 135-138.

[21] C. Haskell-Luevano, E.K. Monck, Agouti-related protein functions as an inverse agonist at a constitutively active brain melanocortin-4 receptor, Regul Pept, 99 (2001) 1-7.

[22] W.A. Nijenhuis, J. Oosterom, R.A. Adan, AgRP(83-132) acts as an inverse agonist on the human melanocortin-4 receptor, Mol Endocrinol, 15 (2001) 164-171.

[23] M.W. Schwartz, S.C. Woods, D. Porte, Jr., R.J. Seeley, D.G. Baskin, Central nervous system control of food intake, Nature, 404 (2000) 661-671.

[24] G.J. Morton, D.E. Cummings, D.G. Baskin, G.S. Barsh, M.W. Schwartz, Central nervous system control of food intake and body weight, Nature, 443 (2006) 289-295.

[25] C.C. Cheung, D.K. Clifton, R.A. Steiner, Proopiomelanocortin neurons are direct targets for leptin in the hypothalamus, Endocrinology, 138 (1997) 4489-4492.

[26] M. van den Top, K. Lee, A.D. Whyment, A.M. Blanks, D. Spanswick, Orexigen-sensitive NPY/AgRP pacemaker neurons in the hypothalamic arcuate nucleus, Nat Neurosci, 7 (2004) 493-494.

[27] A.C. Konner, R. Janoschek, L. Plum, S.D. Jordan, E. Rother, X. Ma, C. Xu, P. Enriori, B. Hampel, G.S. Barsh, C.R. Kahn, M.A. Cowley, F.M. Ashcroft, J.C. Bruning, Insulin action in AgRP-expressing neurons is required for suppression of hepatic glucose production, Cell Metab, 5 (2007) 438-449.

[28] R.D. Cone, Anatomy and regulation of the central melanocortin system, Nat Neurosci, 8 (2005) 571-578.

[29] Y. Zhang, R. Proenca, M. Maffei, M. Barone, L. Leopold, J.M. Friedman, Positional cloning of the mouse obese gene and its human homologue, Nature, 372 (1994) 425-432.

[30] A.A. Butler, R.A. Kesterson, K. Khong, M.J. Cullen, M.A. Pelleymounter, J. Dekoning, M. Baetscher, R.D. Cone, A unique metabolic syndrome causes obesity in the melanocortin-3 receptor-deficient mouse, Endocrinology, 141 (2000) 3518-3521.

[31] Y.S. Lee, L.K. Poh, K.Y. Loke, A novel melanocortin 3 receptor gene (MC3R) mutation associated with severe obesity, J Clin Endocrinol Metab, 87 (2002) 1423-1426.

[32] Y.X. Tao, D.L. Segaloff, Functional characterization of melanocortin-3 receptor variants identify a loss-of-function mutation involving an amino acid critical for G protein-coupled receptor activation, J Clin Endocrinol Metab, 89 (2004) 3936-3942.

[33] Y.X. Tao, Functional characterization of novel melanocortin-3 receptor mutations

identified from obese subjects, Biochim Biophys Acta, 1772 (2007) 1167-1174.

[34] M. Ghamari-Langroudi, I. Cakir, R.N. Lippert, P. Sweeney, M.J. Litt, K.L.J. Ellacott, R.D. Cone, Regulation of energy rheostasis by the melanocortin-3 receptor, Sci Adv, 4 (2018) eaat0866.

[35] D. Huszar, C.A. Lynch, V. Fairchild-Huntress, J.H. Dunmore, Q. Fang, L.R. Berkemeier, W. Gu, R.A. Kesterson, B.A. Boston, R.D. Cone, F.J. Smith, L.A. Campfield, P. Burn, F. Lee, Targeted disruption of the melanocortin-4 receptor results in obesity in mice, Cell, 88 (1997) 131-141.

[36] N. Balthasar, L.T. Dalgaard, C.E. Lee, J. Yu, H. Funahashi, T. Williams, M. Ferreira, V. Tang, R.A. McGovern, C.D. Kenny, L.M. Christiansen, E. Edelstein, B. Choi, O. Boss, C. Aschkenasi, C.Y. Zhang, K. Mountjoy, T. Kishi, J.K. Elmquist, B.B. Lowell, Divergence of melanocortin pathways in the control of food intake and energy expenditure, Cell, 123 (2005) 493-505.

[37] J. Rossi, N. Balthasar, D. Olson, M. Scott, E. Berglund, C.E. Lee, M.J. Choi, D. Lauzon, B.B. Lowell, J.K. Elmquist, Melanocortin-4 receptors expressed by cholinergic neurons regulate energy balance and glucose homeostasis, Cell Metab, 13 (2011) 195-204.

[38] M. Chen, Y.B. Shrestha, B. Podyma, Z. Cui, B. Naglieri, H. Sun, T. Ho, E.A. Wilson, Y.Q. Li, O. Gavrilova, L.S. Weinstein, Gsalpha deficiency in the dorsomedial hypothalamus underlies obesity associated with Gsalpha mutations, J Clin Invest, 127 (2017) 500-510.

[39] C. Vaisse, K. Clement, B. Guy-Grand, P. Froguel, A frameshift mutation in human

MC4R is associated with a dominant form of obesity, Nat Genet, 20 (1998) 113-114.

[40] G.S. Yeo, I.S. Farooqi, S. Aminian, D.J. Halsall, R.G. Stanhope, S. O'Rahilly, A frameshift mutation in MC4R associated with dominantly inherited human obesity, Nat Genet, 20 (1998) 111-112.

[41] W.M. Oldham, H.E. Hamm, Heterotrimeric G protein activation by G-protein-coupled receptors, Nat Rev Mol Cell Biol, 9 (2008) 60-71.

[42] Y.X. Tao, Z.H. Yuan, J. Xie, G protein-coupled receptors as regulators of energy homeostasis, Prog Mol Biol Transl Sci, 114 (2013) 1-43.

[43] S. Offermanns, G-proteins as transducers in transmembrane signalling, Prog Biophys Mol Biol, 83 (2003) 101-130.

[44] K.A. Martemyanov, M. Garcia-Marcos, Making useful gadgets with miniaturized G proteins, J Biol Chem, 293 (2018) 7474-7475.

[45] H. Yang, L. Yang, Targeting cAMP/PKA pathway for glycemic control and type 2 diabetes therapy, J Mol Endocrinol, 57 (2016) R93-R108.

[46] S.L. Ritter, R.A. Hall, Fine-tuning of GPCR activity by receptor-interacting proteins, Nat Rev Mol Cell Biol, 10 (2009) 819-830.

[47] R.T. Dorsam, J.S. Gutkind, G-protein-coupled receptors and cancer, Nat Rev Cancer, 7 (2007) 79-94.

[48] W.E. Miller, R.J. Lefkowitz, Expanding roles for β-arrestins as scaffolds and adapters in GPCR signaling and trafficking, Curr Opin Cell Biol, 13 (2001) 139-145.

[49] A.R.B. Thomsen, B. Plouffe, T.J. Cahill III, A.K. Shukla, J.T. Tarrasch, A.M. Dosey,

A.W. Kahsai, R.T. Strachan, B. Pani, J.P. Mahoney, GPCR-G protein-β-arrestin super-complex mediates sustained G protein signaling, Cell, 166 (2016) 907-919.

[50] M. Luttrell, R.J. Lefkowitz, The role of β-arrestins in the termination and transduction of G-protein-coupled receptor signals, J Cell Sci, 115 (2002) 455-465.

[51] A.R. Rodrigues, H. Almeida, A.M. Gouveia, Intracellular signaling mechanisms of the melanocortin receptors: current state of the art, Cell Mol Life Sci, 72 (2015) 1331-1345.

[52] B. Chai, J.Y. Li, W. Zhang, J.B. Ammori, M.W. Mulholland, Melanocortin-3 receptor activates MAP kinase via PI3 kinase, Regul Pept, 139 (2007) 115-121.

[53] Y. Konda, I. Gantz, J. DelValle, Y. Shimoto, H. Miwa, T. Yamada, Interaction of dual intracellular signaling pathways activated by the melanocortin-3 receptor, J Biol Chem, 269 (1994) 13162-13166.

[54] Z. Yang, Y.X. Tao, Biased signaling initiated by agouti-related peptide through human melanocortin-3 and -4 receptors, Biochim Biophys Acta, 1862 (2016) 1485-1494.

[55] T.R. Büch, D. Heling, E. Damm, T. Gudermann, A. Breit, Pertussis toxin-sensitive signaling of melanocortin-4 receptors in hypothalamic GT1-7 cells defines agouti-related protein as a biased agonist, J Biol Chem, 284 (2009) 26411-26420.

[56] E.A. Newman, B.X. Chai, W. Zhang, J.Y. Li, J.B. Ammori, M.W. Mulholland, Activation of the melanocortin-4 receptor mobilizes intracellular free calcium in immortalized hypothalamic neurons, J Surg Res, 132 (2006) 201-207.

[57] B. Chai, J.Y. Li, W. Zhang, E. Newman, J. Ammori, M.W. Mulholland, Melanocortin-4 receptor-mediated inhibition of apoptosis in immortalized hypothalamic neurons via mitogen-activated protein kinase, Peptides, 27 (2006) 2846-2857.

[58] D. Daniels, C.S. Patten, J.D. Roth, D.K. Yee, S.J. Fluharty, Melanocortin receptor signaling through mitogen-activated protein kinase in vitro and in rat hypothalamus, Brain Res, 986 (2003) 1-11.

[59] A. Vongs, N.M. Lynn, C.I. Rosenblum, Activation of MAP kinase by MC4-R through PI3 kinase, Regul Pept, 120 (2004) 113-118.

[60] E. Damm, T.R. Buech, T. Gudermann, A. Breit, Melanocortin-induced PKA activation inhibits AMPK activity via ERK-1/2 and LKB-1 in hypothalamic GT1-7 cells, Mol Endocrinol, 26 (2012) 643-654.

[61] A.R. Rodrigues, H. Almeida, A.M. Gouveia, Melanocortin 5 receptor signaling and internalization: role of MAPK/ERK pathway and β-arrestins 1/2, Mol Cell Endocrinol, 361 (2012) 69-79.

[62] H. Shinyama, H. Masuzaki, H. Fang, J.S. Flier, Regulation of melanocortin-4 receptor signaling: agonist-mediated desensitization and internalization, Endocrinology, 144 (2003) 1301-1314.

[63] A. Breit, K. Wolff, H. Kalwa, H. Jarry, T. Buch, T. Gudermann, The natural inverse agonist agouti-related protein induces arrestin-mediated endocytosis of melanocortin-3 and -4 receptors, J Biol Chem, 281 (2006) 37447-37456.

[64] L.A. Lotta, J. Mokrosiński, E.M. de Oliveira, C. Li, S.J. Sharp, J. Luan, B. Brouwers, V. Ayinampudi, N. Bowker, N. Kerrison, Human gain-of-function MC4R variants show signaling bias and protect against obesity, Cell, 177 (2019) 597-607. e599.

[65] Y. Minokoshi, T. Alquier, N. Furukawa, Y.B. Kim, A. Lee, B. Xue, J. Mu, F. Foufelle, P. Ferre, M.J. Birnbaum, B.J. Stuck, B.B. Kahn, AMP-kinase regulates food intake by

responding to hormonal and nutrient signals in the hypothalamus, Nature, 428 (2004) 569-574.

[66] G.M. Sutton, B. Duos, L.M. Patterson, H.R. Berthoud, Melanocortinergic modulation of cholecystokinin-induced suppression of feeding through extracellular signal-regulated kinase signaling in rat solitary nucleus, Endocrinology, 146 (2005) 3739-3747.

[67] A. Traboulsie, J. Chemin, M. Chevalier, J.F. Quignard, J. Nargeot, P. Lory, Subunit-specific modulation of T-type calcium channels by zinc, J Physiol, 578 (2007) 159-171.

[68] A. Draguhn, T.A. Verdorn, M. Ewert, P.H. Seeburg, B. Sakmann, Functional and molecular distinction between recombinant rat $GABA_A$ receptor subtypes by Zn^{2+}, Neuron, 5 (1990) 781-788.

[69] B. Laube, J. Kuhse, N. Rundström, J. Kirsch, V. Schmieden, H. Betz, Modulation by zinc ions of native rat and recombinant human inhibitory glycine receptors, J Physiol, 483 (1995) 613-619.

[70] A. Strasser, H.-J. Wittmann, E.H. Schneider, R. Seifert, Modulation of GPCRs by monovalent cations and anions, Naunyn Schmiedebergs Arch Pharmacol, 388 (2015) 363-380.

[71] K. Młyniec, N. Singewald, B. Holst, G. Nowak, GPR39 Zn^{2+}-sensing receptor: A new target in antidepressant development?, J Affect Disord, 174 (2015) 89-100.

[72] T.G. Smart, X. Xie, B.J. Krishek, Modulation of inhibitory and excitatory amino acid receptor ion channels by zinc, Prog Neurobiol, 42 (1994) 393-441.

[73] S.Y. Assaf, S.H. Chung, Release of endogenous Zn^{2+} from brain tissue during activity,

Nature, 308 (1984) 734-736.

[74] B. Holst, C.E. Elling, T.W. Schwartz, Metal ion-mediated agonism and agonist enhancement in melanocortin MC1 and MC4 receptors, J Biol Chem, 277 (2002) 47662-47670.

[75] L. Storjohann, B. Holst, T.W. Schwartz, Molecular mechanism of Zn^{2+} agonism in the extracellular domain of GPR39, FEBS Lett, 582 (2008) 2583-2588.

[76] B. Holst, T.W. Schwartz, Molecular mechanism of agonism and inverse agonism in the melanocortin receptors: Zn^{2+} as a structural and functional probe, Ann N Y Acad Sci, 994 (2003) 1-11.

[77] A. Mathie, G.L. Sutton, C.E. Clarke, E.L. Veale, Zinc and copper: pharmacological probes and endogenous modulators of neuronal excitability, Pharmacol Ther, 111 (2006) 567-583.

[78] A. Myari, G. Malandrinos, Y. Deligiannakis, J.C. Plakatouras, N. Hadjiliadis, Z. Nagy, I. Sovago, Interaction of Cu^{2+} with His–Val–His and of Zn^{2+} with His–Val–Gly–Asp, two peptides surrounding metal ions in Cu, Zn-superoxide dismutase enzyme, J Inorg Biochem, 85 (2001) 253-261.

[79] I.N. Sharonova, V.S. Vorobjev, H.L. Haas, Interaction between copper and zinc at GABAA receptors in acutely isolated cerebellar Purkinje cells of the rat, Br J Pharmacol, 130 (2000) 851.

[80] P.Q. Trombley, G.M. Shepherd, Differential modulation by zinc and copper of amino acid receptors from rat olfactory bulb neurons, J Neurophysiol, 76 (1996) 2536-2546.

[81] T. Narahashi, J.Y. Ma, O. Arakawa, E. Reuveny, M. Nakahiro, GABA receptor-channel

complex as a target site of mercury, copper, zinc, and lanthanides, Cell Mol Neurobiol, 14 (1994) 599-621.

[82] R. Link, S. Veiksina, M.J. Tahk, T. Laasfeld, P. Paiste, S. Kopanchuk, A. Rinken, The constitutive activity of melanocortin‐4 receptors in cAMP pathway is allosterically modulated by zinc and copper ions, J Neurochem, (2019) e14933.

[83] I. Gantz, Y. Konda, T. Tashiro, Y. Shimoto, H. Miwa, G. Munzert, S.J. Watson, J. DelValle, T. Yamada, Molecular cloning of a novel melanocortin receptor, J Biol Chem, 268 (1993) 8246-8250.

[84] K.G. Mountjoy, M.T. Mortrud, M.J. Low, R.B. Simerly, R.D. Cone, Localization of the melanocortin-4 receptor (MC4-R) in neuroendocrine and autonomic control circuits in the brain, Mol Endocrinol, 8 (1994) 1298-1308.

[85] T. Kishi, C.J. Aschkenasi, C.E. Lee, K.G. Mountjoy, C.B. Saper, J.K. Elmquist, Expression of melanocortin 4 receptor mRNA in the central nervous system of the rat, J Comp Neurol, 457 (2003) 213-235.

[86] M. van der Kraan, J.B. Tatro, M.L. Entwistle, J.H. Brakkee, J.P. Burbach, R.A. Adan, W.H. Gispen, Expression of melanocortin receptors and pro-opiomelanocortin in the rat spinal cord in relation to neurotrophic effects of melanocortins, Brain Res Mol Brain Res, 63 (1999) 276-286.

[87] R. Poggioli, A.V. Vergoni, A. Bertolini, ACTH-(1-24) and alpha-MSH antagonize feeding behavior stimulated by kappa opiate agonists, Peptides, 7 (1986) 843-848.

[88] A.V. Vergoni, R. Poggioli, A. Bertolini, Corticotropin inhibits food intake in rats,

Neuropeptides, 7 (1986) 153-158.

[89] H. Huang, W. Wang, Y.X. Tao, Pharmacological chaperones for the misfolded melanocortin-4 receptor associated with human obesity, Biochim Biophys Acta, (2017) 2496-2507.

[90] Y.X. Tao, P.M. Conn, Chaperoning G protein-coupled receptors: From cell biology to therapeutics, Endocr Rev, 35 (2014) 602-647.

[91] Y.X. Tao, H. Huang, Ipsen 5i is a novel potent pharmacoperone for intracellularly retained melanocortin-4 receptor mutants, Front Endocrinol, 5 (2014) 131.

[92] A. Hinney, T. Bettecken, P. Tarnow, H. Brumm, K. Reichwald, P. Lichtner, A. Scherag, T.T. Nguyen, P. Schlumberger, W. Rief, C. Vollmert, T. Illig, H.E. Wichmann, H. Schafer, M. Platzer, H. Biebermann, T. Meitinger, J. Hebebrand, Prevalence, spectrum, and functional characterization of melanocortin-4 receptor gene mutations in a representative population-based sample and obese adults from Germany, J Clin Endocrinol Metab, 91 (2006) 1761-1769.

[93] C. Vaisse, K. Clement, E. Durand, S. Hercberg, B. Guy-Grand, P. Froguel, Melanocortin-4 receptor mutations are a frequent and heterogeneous cause of morbid obesity, J Clin Invest, 106 (2000) 253-262.

[94] X.L. Mo, R. Yang, Y.X. Tao, Functions of transmembrane domain 3 of human melanocortin-4 receptor, J Mol Endocrinol, 49 (2012) 221-235.

[95] A.L. Steiner, D.M. Kipnis, R. Utiger, C. Parker, Radioimmunoassay for the measurement of adenosine 3',5'-cyclic phosphate, Proc Natl Acad Sci U S A, 64 (1969) 367-373.

[96] Y.X. Tao, H. Huang, Z.Q. Wang, F. Yang, J.N. Williams, G.V. Nikiforovich, Constitutive activity of neural melanocortin receptors, Methods Enzymol, 484 (2010) 267-279.

[97] Y.X. Tao, D.L. Segaloff, Functional characterization of melanocortin-4 receptor mutations associated with childhood obesity, Endocrinology, 144 (2003) 4544-4551.

[98] C. Chen, H. Okayama, High-efficiency transformation of mammalian cells by plasmid DNA, Mol Cell Biol, 7 (1987) 2745-2752.

[99] X.L. Mo, Y.X. Tao, Activation of MAPK by inverse agonists in six naturally occurring constitutively active mutant human melanocortin-4 receptors, Biochim Biophys Acta, 1832 (2013) 1939-1948.

[100] K. Clément, H. Biebermann, I.S. Farooqi, L.H. Van der Ploeg, B. Wolters, C. Poitou, L. Puder, F. Fiedorek, K.M. Gottesdiener, G. Kleinau, MC4R agonism promotes durable weight loss in patients with leptin receptor deficiency, Nat Med, 24 (2018) 551-555.

[101] J. Yu, L.E. Gimenez, C.C. Hernandez, Y. Wu, A.H. Wein, G.W. Han, K. McClary, S.R. Mittal, K. Burdsall, B. Stauch, Determination of the melanocortin-4 receptor structure identifies Ca^{2+} as a cofactor for ligand binding, Science, 368 (2020) 428-433.

[102] C.B. Pert, S.H. Snyder, Opiate receptor binding of agonists and antagonists affected differentially by sodium, Mol Pharmacol, 10 (1974) 868-879.

[103] C.B. Pert, S.H. Snyder, Opiate receptor: demonstration in nervous tissue, Science, 179 (1973) 1011-1014.

[104] G.W. Pasternak, A.M. Snowman, S.H. Snyder, Selective enhancement of [^{3}H] opiate agonist binding by divalent cations, Mol Pharmacol, 11 (1975) 735-744.

[105] C. Silve, C. Petrel, C. Leroy, H. Bruel, E. Mallet, D. Rognan, M. Ruat, Delineating a

Ca^{2+} binding pocket within the venus flytrap module of the human calcium-sensing receptor, J Biol Chem, 280 (2005) 37917-37923.

[106] V. Katritch, G. Fenalti, E.E. Abola, B.L. Roth, V. Cherezov, R.C. Stevens, Allosteric sodium in class A GPCR signaling, Trends Biochem Sci, 39 (2014) 233-244.

[107] G. Swaminath, T.W. Lee, B. Kobilka, Identification of an allosteric binding site for Zn^{2+} on the β_2 adrenergic receptor, J Biol Chem, 278 (2003) 352-356.

[108] G. Swaminath, J. Steenhuis, B. Kobilka, T.W. Lee, Allosteric modulation of β_2-adrenergic receptor by Zn^{2+}, Mol Pharmacol, 61 (2002) 65-72.

[109] G. Satała, B. Duszyńska, K. Stachowicz, A. Rafalo, B. Pochwat, C. Luckhart, P.R. Albert, M. Daigle, K.F. Tanaka, R. Hen, Concentration-dependent dual mode of Zn action at serotonin 5-HT1A receptors: in vitro and in vivo studies, Mol Neurobiol, 53 (2016) 6869-6881.

[110] A. Stojanovic, J. Stitham, J. Hwa, Critical role of transmembrane segment zinc binding in the structure and function of rhodopsin, J Biol Chem, 279 (2004) 35932-35941.

[111] S. Gleim, A. Stojanovic, E. Arehart, D. Byington, J. Hwa, Conserved rhodopsin intradiscal structural motifs mediate stabilization: effects of zinc, Biochemistry, 48 (2009) 1793-1800.

[112] C.E. Elling, K. Thirstrup, B. Holst, T.W. Schwartz, Conversion of agonist site to metal-ion chelator site in the beta(2)-adrenergic receptor, Proc Natl Acad Sci U S A, 96 (1999) 12322-12327.

[113] J.M. Berg, Y. Shi, The galvanization of biology: a growing appreciation for the roles of zinc, Science, 271 (1996) 1081-1085.

[114] B. Trzaskowski, L. Adamowicz, P.A. Deymier, A theoretical study of zinc (II) interactions with amino acid models and peptide fragments, J. Biol. Inorg. Chem., 13 (2008) 133-137.

[115] M.D. Ericson, C.J. Lensing, K.A. Fleming, K.N. Schlasner, S.R. Doering, C. Haskell-Luevano, Bench-top to clinical therapies: A review of melanocortin ligands from 1954 to 2016, Biochim Biophys Acta, (2017).

[116] Y.X. Tao, Melanocortin receptors, Biochim Biophys Acta, 1863 (2017) 2411-2413.

[117] T.K. Sawyer, P.J. Sanfilippo, V.J. Hruby, M.H. Engel, C.B. Heward, J.B. Burnett, M.E. Hadley, 4-Norleucine, 7-D-phenylalanine-a-melanocyte-stimulating hormone: a highly potent a-melanotropin with ultralong biological activity, Proc Natl Acad Sci U S A, 77 (1980) 5754-5758.

[118] I.K. Sebhat, W.J. Martin, Z. Ye, K. Barakat, R.T. Mosley, D.B. Johnston, R. Bakshi, B. Palucki, D.H. Weinberg, T. MacNeil, R.N. Kalyani, R. Tang, R.A. Stearns, R.R. Miller, C. Tamvakopoulos, A.M. Strack, E. McGowan, D.E. Cashen, J.E. Drisko, G.J. Hom, A.D. Howard, D.E. MacIntyre, L.H. van der Ploeg, A.A. Patchett, R.P. Nargund, Design and pharmacology of N-[(3R)-1,2,3,4-tetrahydroisoquinolinium- 3-ylcarbonyl]-(1R)-1-(4-chlorobenzyl)- 2-[4-cyclohexyl-4-(1H-1,2,4-triazol- 1-ylmethyl)piperidin-1-yl]-2-oxoethylamine (1), a potent, selective, melanocortin subtype-4 receptor agonist, J Med Chem, 45 (2002) 4589-4593.

[119] Y.X. Tao, Mutations in melanocortin-4 receptor and human obesity, Prog Mol Biol Transl Sci, 88 (2009) 173-204.

[120] A. Hinney, A.L. Volckmar, N. Knoll, Melanocortin-4 receptor in energy homeostasis

and obesity pathogenesis, Prog Mol Biol Transl Sci, 114 (2013) 147-191.

[121] H. Watanobe, H.B. Schioth, J. Izumi, Pivotal roles of alpha-melanocyte-stimulating hormone and the melanocortin 4 receptor in leptin stimulation of prolactin secretion in rats, J Neurochem, 85 (2003) 338-347.

[122] K. Khong, S.E. Kurtz, R.L. Sykes, R.D. Cone, Expression of functional melanocortin-4 receptor in the hypothalamic GT1-1 cell line, Neuroendocrinology, 74 (2001) 193-201.

[123] J. Roa, A.E. Herbison, Direct regulation of GnRH neuron excitability by arcuate nucleus POMC and NPY neuron neuropeptides in female mice, Endocrinology, 153 (2012) 5587-5599.

[124] Y.X. Tao, Molecular mechanisms of the neural melanocortin receptor dysfunction in severe early onset obesity, Mol Cell Endocrinol, 239 (2005) 1-14.

[125] A. Ringholm, R. Fredriksson, N. Poliakova, Y.L. Yan, J.H. Postlethwait, D. Larhammar, H.B. Schioth, One melanocortin 4 and two melanocortin 5 receptors from zebrafish show remarkable conservation in structure and pharmacology, J Neurochem, 82 (2002) 6-18.

[126] J.M. Cerda-Reverter, A. Ringholm, H.B. Schioth, R.E. Peter, Molecular cloning, pharmacological characterization, and brain mapping of the melanocortin 4 receptor in the goldfish: involvement in the control of food intake, Endocrinology, 144 (2003) 2336-2349.

[127] Y. Kobayashi, K. Tsuchiya, T. Yamanome, H.B. Schioth, H. Kawauchi, A. Takahashi, Food deprivation increases the expression of melanocortin-4 receptor in the liver of barfin flounder, *Verasper moseri*, Gen Comp Endocrinol, 155 (2008) 280-287.

[128] J.T. Li, Z. Yang, H.P. Chen, C.H. Zhu, S.P. Deng, G.L. Li, Y.X. Tao, Molecular cloning, tissue distribution, and pharmacological characterization of melanocortin-4 receptor in spotted scat, *Scatophagus argus*, Gen Comp Endocrinol, 230-231 (2016) 143 -152.

[129] L. Li, Z. Yang, Y.P. Zhang, S. He, X.F. Liang, Y.X. Tao, Molecular cloning, tissue distribution, and pharmacological characterization of melanocortin-4 receptor in grass carp (*Ctenopharyngodon idella*), Domest Anim Endocrinol, 59 (2017) 140-151.

[130] T.L. Yi, L.K. Yang, G.L. Ruan, D.Q. Yang, Y.X. Tao, Melanocortin-4 receptor in swamp eel (*Monopterus albus*): cloning, tissue distribution, and pharmacology, Gene, 678 (2018) 79-89.

[131] Y.Z. Rao, R. Chen, Y. Zhang, Y.X. Tao, Orange-spotted grouper melanocortin-4 receptor: modulation of signaling by MRAP2, Gen Comp Endocrinol, 284 (2019) 113234.

[132] A.C. Aspiras, N. Rohner, B. Martineau, R.L. Borowsky, C.J. Tabin, Melanocortin 4 receptor mutations contribute to the adaptation of cavefish to nutrient-poor conditions, Proc Natl Acad Sci U S A, 112 (2015) 9668-9673.

[133] Y. Song, R.D. Cone, Creation of a genetic model of obesity in a teleost, FASEB J, 21 (2007) 2042-2049.

[134] J.M. Cerda-Reverter, H.B. Schioth, R.E. Peter, The central melanocortin system regulates food intake in goldfish, Regul Pept, 115 (2003) 101-113.

[135] J. Schjolden, H.B. Schiöth, D. Larhammar, S. Winberg, E.T. Larson, Melanocortin peptides affect the motivation to feed in rainbow trout (*Oncorhynchus mykiss*), Gen Comp Endocrinol, 160 (2009) 134-138.

[136] K.P. Lampert, C. Schmidt, P. Fischer, J.N. Volff, C. Hoffmann, J. Muck, M.J. Lohse,

M.J. Ryan, M. Schartl, Determination of onset of sexual maturation and mating behavior by melanocortin receptor 4 polymorphisms, Curr Biol, 20 (2010) 1729-1734.

[137] C.C. Smith, R.M. Harris, K.P. Lampert, M. Schartl, H.A. Hofmann, M.J. Ryan, Copy number variation in the melanocortin 4 receptor gene and alternative reproductive tactics the swordtail Xiphophorus multilineatus, Environ Biol Fishes, 98 (2015) 23-33.

[138] D.N. Jiang, J.T. Li, Y.X. Tao, H.P. Chen, S.P. Deng, C.H. Zhu, G.L. Li, Effects of melanocortin-4 receptor agonists and antagonists on expression of genes related to reproduction in spotted scat, Scatophagus argus, J Comp Physiol B, 187 (2017) 603-612.

[139] K.J. Livak, T.D. Schmittgen, Analysis of relative gene expression data using real-time quantitative PCR and the $2^{-\Delta\Delta CT}$ method, Methods, 25 (2001) 402-408.

[140] X. Qi, W. Zhou, D. Lu, Q. Wang, H. Zhang, S. Li, X. Liu, Y. Zhang, H. Lin, Sexual dimorphism of steroidogenesis regulated by GnIH in the goldfish, Carassius auratus, Biol Reprod, 88 (2013) 89, 81-87.

[141] R.M. Dores, R.L. Londraville, J. Prokop, P. Davis, N. Dewey, N. Lesinski, Molecular evolution of GPCRs: Melanocortin/melanocortin receptors, J Mol Endocrinol, 52 (2014) T29-42.

[142] R. Schwyzer, ACTH: a short introductory review, Ann N Y Acad Sci, 297 (1977) 3-26.

[143] Z.C. Fan, Y.X. Tao, Functional characterization and pharmacological rescue of melanocortin-4 receptor mutations identified from obese patients, J Cell Mol Med, 13 (2009) 3268-3282.

[144] H. Huang, Y.X. Tao, A small molecule agonist THIQ as a novel pharmacoperone for

intracellularly retained melanocortin-4 receptor mutants, Int J Biol Sci, 10 (2014) 817-824.

[145] S.X. Wang, Z.C. Fan, Y.X. Tao, Functions of acidic transmembrane residues in human melanocortin-3 receptor binding and activation, Biochem Pharmacol, 76 (2008) 520-530.

[146] A. Jangprai, S. Boonanuntanasarn, G. Yoshizaki, Characterization of melanocortin 4 receptor in Snakeskin Gourami and its expression in relation to daily feed intake and short-term fasting, Gen Comp Endocrinol, 173 (2011) 27-37.

[147] R. Wei, D. Yuan, C. Zhou, T. Wang, F. Lin, H. Chen, H. Wu, Z. Xin, S. Yang, D. Chen, Y. Wang, J. Liu, Y. Gao, Z. Li, Cloning, distribution and effects of fasting status of melanocortin 4 receptor (MC4R) in *Schizothorax prenanti*, Gene, 532 (2013) 100-107.

[148] P. Tarnow, T. Schoneberg, H. Krude, A. Gruters, H. Biebermann, Mutationally induced disulfide bond formation within the third extracellular loop causes melanocortin 4 receptor inactivation in patients with obesity, J Biol Chem, 278 (2003) 48666-48673.

[149] Z.X. Li, B.W. Liu, Z.G. He, H.B. Xiang, Melanocortin-4 receptor regulation of pain, Biochim Biophys Acta, (2017) 2515-2522.

[150] K.Q. Zhang, Z.S. Hou, H.S. Wen, Y. Li, X. Qi, W.J. Li, Y.X. Tao, Melanocortin-4 Receptor in Spotted Sea Bass, *Lateolabrax maculatus*: Cloning, Tissue Distribution, Physiology, and Pharmacology, Front Endocrinol, 10 (2019) 705.

[151] T. Haitina, J. Klovins, J. Andersson, R. Fredriksson, M.C. Lagerstrom, D. Larhammar, E.T. Larson, H.B. Schioth, Cloning, tissue distribution, pharmacology and three-dimensional modelling of melanocortin receptors 4 and 5 in rainbow trout suggest close evolutionary relationship of these subtypes, Biochem J, 380 (2004) 475-486.

[152] J. Klovins, T. Haitina, D. Fridmanis, Z. Kilianova, I. Kapa, R. Fredriksson, N. Gallo-Payet, H.B. Schioth, The melanocortin system in Fugu: determination of POMC/AGRP/MCR gene repertoire and synteny, as well as pharmacology and anatomical distribution of the MCRs, Mol Biol Evol, 21 (2004) 563-579.

[153] M. Zhang, K.P. Tong, V. Fremont, J. Chen, P. Narayan, D. Puett, B.D. Weintraub, M.W. Szkudlinski, The extracellular domain suppresses constitutive activity of the transmembrane domain of the human TSH receptor: implications for hormone-receptor interaction and antagonist design, Endocrinology, 141 (2000) 3514-3517.

[154] S. Nishi, K. Nakabayashi, B. Kobilka, A.J. Hsueh, The ectodomain of the luteinizing hormone receptor interacts with exoloop 2 to constrain the transmembrane region. Studies using chimeric human and fly receptors, J Biol Chem, 277 (2002) 3958-3964.

[155] K.J. Paavola, J.R. Stephenson, S.L. Ritter, S.P. Alter, R.A. Hall, The N terminus of the adhesion G protein-coupled receptor GPR56 controls receptor signaling activity, J Biol Chem, 286 (2011) 28914-28921.

[156] Y.X. Tao, Constitutive activity in melanocortin-4 receptor: biased signaling of inverse agonists, Adv Pharmacol, 70 (2014) 135-154.

[157] Y.X. Tao, Constitutive activation of G protein-coupled receptors and diseases: Insights into mechanism of activation and therapeutics, Pharmacol Ther, 120 (2008) 129-148.

[158] S. Srinivasan, C. Lubrano-Berthelier, C. Govaerts, F. Picard, P. Santiago, B.R. Conklin, C. Vaisse, Constitutive activity of the melanocortin-4 receptor is maintained by its N-terminal domain and plays a role in energy homeostasis in humans, J Clin Invest,

114 (2004) 1158-1164.